Utah Water Research Laboratory

A Spatially-Distributed Hydrologic Model for a Small Arid Mountain Watershed

Thomas H. Jackson
David G. Tarboton
Keith R. Cooley

Working Paper WP-96-HWR-DGT/002

May 1996.

Utah Water Research Laboratory, Utah State University, Logan UT 84322-8200, USA
(801)-797-3172: FAX:(801)-797-3663

A SPATIALLY-DISTRIBUTED HYDROLOGIC MODEL FOR A SMALL ARID MOUNTAIN WATERSHED

by

Thomas H. Jackson,
Brown & Root, Inc.

David G. Tarboton,
Utah State University

Keith R. Cooley,
USDA ARS Northwest Watershed Research Center

ABSTRACT

A distributed water balance model was developed as a part of an intensive field study to simulate the snowmelt-driven hydrologic response of a small mountain watershed using measured values of solar radiation, wind speed, air temperature, relative humidity and precipitation as input.

Snowmelt and evapotranspiration were modeled with point energy balances, written in terms of the snow surface and soil surface temperatures, respectively, corrected for local topographic characteristics and snow drifting. Meltwater was routed to the basin outlet as topography-driven, saturated subsurface flow, with all flow in excess of local transmissivity taken as surface runoff.

The model was calibrated with 1985-6 data and verified with 1992-3 data at Upper Sheep Creek, in Owyhee County, Idaho. It accurately simulated the spatial pattern of snow accumulation and ablation, and reproduced the timing and magnitude of peak basin snowmelt runoff. Runoff from rainfall on dry soil was not well modeled.

1. INTRODUCTION

This paper describes the distributed hydrologic model we developed to study the water budget of a small mountain catchment in the Reynolds Creek Experimental Watershed, maintained by the Agricultural Research Service (ARS) in Owyhee County, Idaho. The site for model development, shown in Figures 1 and 2, was Upper Sheep Creek, a 26 hectare headwater catchment drained by an intermittent stream with year-to-year yield dependent on the winter snow pack (Flerchinger et al, 1992).

Our modeling effort combined traditional water budget and data gathering efforts with an attempt to develop a simple distributed watershed model that would be capable of reproducing the changes in the spatial pattern of moisture storage in the watershed over time as well as the outflow hydrograph. Following recent developments in distributed watershed modeling (Troendle, 1985; Troch et al.,1993, Band and Wood, 1988; Paniconi and Wood, 1993; Moore, 1991; Grayson and Moore 1992a,b; Wigmosta et al., 1994, Beven, 1992; Beven and Binley, 1992), we superimposed our model on a grid-based digital elevation model (DEM) of catchment topography. This made it possible to account for the effects of local elevation, slope, and aspect on energy and mass balances with sufficient resolution to simulate hydrologic processes at the hillslope scale. By maintaining a mass balance for each DEM grid cell, and accounting for flux between cells, we ensured that our overall water budget for the catchment would be consistent with our representation of local processes.

We designed our model to be a shell program for managing data gathered throughout the watershed in a DEM-based geographic information system (GIS). This allowed the correlation of snow water equivalent (SWE) depths and melt rates measured in the field with topographic attributes determined from the DEM.

Another goal in model development was to study how the relative importance of the key hydrologic

fluxes varied during the season in each part of the watershed. A strong motivation for this interest continues to be the prediction of overall watershed yield at the seasonal and event-based time scales using a single model. In addition, we feel that comparing measured moisture stores and fluxes with simulated values within the catchment on a distributed basis provides a more robust test of our equations than matching outflow hydrographs can, and will eventually lead to a better understanding of the hydrologic processes involved in arid mountain watersheds.

In our model, these processes are represented in terms of state variables at each grid point in the DEM. This allows us to account for SWE (if present), surface energy content, and subsurface moisture deficit at each time step. Changes in the state variables of each cell are accounted for with physically-based equations and energy and mass balances using measured inputs of radiation, precipitation, air temperature, wind speed, and relative humidity. One simplification introduced was that meltwater and rainfall made available at the surface of each cell in a time step was immediately used to satisfy the subsurface moisture deficit, without detention in an unsaturated zone.

Modeling was carried out with a six hour time step, which was fine enough to resolve the diurnal cycles of radiation and temperature that play an important role in the timing of snowmelt inputs and evapotranspiration outputs. This was also a practical time step for modeling subsurface travel times which are in the range of a week to a year. This emphasized interflow and total runoff, and eliminated the necessity for routing overland flow, which seldom has a significant effect on the magnitude of the peak discharge in the small watershed studied.

The model was calibrated with data taken in the Upper Sheep Creek watershed during the 1985-6 snow season and tested against data from the 1992-3 snow season including biweekly distributed measurements

of snow depth and continuous field measurements of climatological inputs, snowmelt and stream flow, as described in Section 3 of this paper.

The test year runs indicated that the model could reproduce the changes in the spatial distribution of surface moisture storage in the watershed over the season, as indicated by snow accumulation patterns, and the basic timing of total watershed response, as indicated by watershed outflow hydrographs. As would be expected, the lack of an unsaturated zone component in the model resulted in a poor simulation of summer season rainfall on dry soil.

In this paper we present the main components of the model, starting with an overview of the DEM grid structure, followed by a description of the mass balance and the snowmelt and ET energy balance models. We then describe how the component parts were combined to simulate the total distributed watershed response and review the application of the model at Upper Sheep Creek. A more detailed description of the model structure and subroutines, and details of its application in the Upper Sheep Creek watershed is presented by Jackson (1994).

2. MODEL STRUCTURE

2.1 Overview

Each node of the DEM grid corresponds to the center of a grid cell which serves as a control volume for surface and subsurface energy and mass balances. The cells are characterized by elevation, slope, aspect, type of vegetative cover, and average values of soil porosity and permeability. These properties

are either extracted from the DEM, or estimated from physical attributes of the site as determined from soil and vegetation maps, remotely sensed data, and field measurements.

The scale of the DEM grid determines the hydrologic processes that can be modeled explicitly. In our application, the cells are 30.48 meters on a side, coinciding with the 100-foot ARS grid on which an extensive series of snow depth and melt rate measurements have been recorded. This resolution is sufficient to resolve the channel network identified as blue lines on 1:24,000 scale topographic maps, but processes that occur at scales smaller than the grid scale need to be parameterized. Macropore flow, for example, is parameterized in terms of an effective saturated hydraulic conductivity.

To account for the component hydrologic processes of the water budget in a physically meaningful manner, an energy and water balance is maintained for each cell in the watershed at each time step, accounting for the fluxes and storage components of the budget with dimensionally consistent equations. A list of the flux and storage components accounted for in the model is presented in Table 1.

The solution of the mass and energy balances gives the state variables for the time step, i.e., W, the SWE storage *on top of*, and D, the moisture deficit *within* each cell. Surface and subsurface moisture stores are linked by downward vertical fluxes of snowmelt and infiltration. The upward flux of evapotranspiration depletes subsurface storage (increases D) when W is zero.

The mass balances for the cells of the model are independent of each other in terms of the vertical fluxes but are linked in terms of lateral subsurface flows. Following the concept of a topography-driven model (Beven and Wood, 1983; Wood et al., 1988), sub-surface flow gradients are assumed to follow overlying topography, so that contributing areas for surface and subsurface flows are the same at each cell. This implies a well developed watershed without abrupt subsurface discontinuities. Flows and moisture deficits simulated by the model can be expected to deviate from measured values to the extent that

the weathered basalt subsurface structure of the study site results in hydraulic gradients that differ from topographic gradients.

The storage of energy in the snow column and the thermally active soil layer beneath it are associated with the state variable U. The calculation of the energy content at each time step allows the calculation of a soil or snow surface *skin-temperature* and enables the calculation of snowmelt, sublimation and evapotranspiration in a physically meaningful manner.

To account for the availability of moisture for vertical infiltration, the snowmelt module uses SWE (W) and albedo as state variables to describe the snow pack. An energy balance is used to model changes in the snow pack at each DEM cell by accounting for fluxes of net short- and long wave radiation, latent and sensible heat transfer, ground heat conductance, and advective heat transfer from incoming rain and snow.

2.2 Grid discretization

A variety of DEM types have been applied for watershed modeling (Moore et al, 1991). The grid-based DEM used in our study represents basin topography with a discrete number of nodes, as shown schematically in Figure 3. Each node is treated as the center of a "cell", or control volume for the energy and mass balances used to represent the key hydrologic processes in the watershed. The vertical transfers of moisture between the atmosphere and the surface and between the surface and subsurface components of each cell are independent.

The mass balances for the cells are linked horizontally by the DEM. The quantity of moisture transferred horizontally between cells is proportional to the surface gradient, which is estimated from the DEM grid in a discrete number of directions. Once a set of flow directions and gradients is determined

for each cell (see Figure 3), its discharge can be routed towards the basin outlet using one of the methods that has been developed for DEM models (O'Callaghan and Mark, 1984; Band, 1986; Jenson and Dominque, 1988).

Following Quinn et al (1991), we employed a multiple direction algorithm in which a cell's contributing area (and flow) is distributed to each down-slope neighbor in proportion to the slope calculated between DEM nodes. The multiple direction flow algorithm allows for more realistic modeling of variable saturated areas but requires the watershed boundaries to be delineated, and a watershed mask must be used to prevent the spreading of contributing areas across ridge lines (see Jackson, 1994, for details).

2.3 Subsurface Water Budget

The distributed watershed model is built up from the water budgets for each cell in the DEM. The subsurface water budget for each cell is written in terms of the deficit, D [m] as:

$$\Delta x^2 \frac{\Delta D}{\Delta t} = Q(t) - I(t) - SF(t) \qquad (1)$$

where Δx is the grid spacing, Q is lateral subsurface outflow, I is lateral subsurface inflow, and SF is the net surface flux, consisting of infiltration from rain or snowmelt minus evapotranspiration, calculated independently for each cell. The deficit, D, is defined as the depth of water that would have to be added to completely saturate the cell. Conceptually, $D = z_s n$, where z_s is the depth to the water table and n the effective porosity of the unsaturated zone. Figure 4 illustrates the various terms in equation

(1).

Subsurface inflow and outflow are calculated as the product of transmissivity and ground surface slope, T*S. Cell transmissivity, T, is obtained by integrating the hydraulic conductivity from the water table surface to the bottom of the aquifer. We use the parameterization, similar to TOPMODEL, that hydraulic conductivity decreases exponentially with depth (Beven and Kirkby, 1979, Kirkby, 1986). This leads to an expression for cell transmissivity in terms of the moisture deficit:

$$T(z_s) = \int_{z_s}^{\infty} k(z)dz = \frac{k_s}{f}.e^{-f.z_s} = \frac{k_s}{f}\, e^{-f\,D/n} \qquad \textbf{(2)}$$

where z_s is the depth to the water table, k_s is the surface saturated hydraulic conductivity, and f is a parameter quantifying the exponential decrease of hydraulic conductivity with depth. We recognize that strict interpretation of exponentially decreasing conductivity is rather restrictive. More conceptually k_s and f can be interpreted as parameters characterizing a probability distribution of hydraulic conductivity independent of depth, assuming that the least conductive layers are preferentially saturated. Alternatively k_s and f can simply be thought of as location and sensitivity parameters respectively. f characterizes the sensitivity of outflow to changes in subsurface moisture storage within a grid cell, and the ratio k_s/f gives the maximum groundwater outflow for saturated conditions (deficit = 0).

Surface slope, S, is determined for each cell in the direction of the eight surrounding cells, as discussed earlier, and flow is apportioned in all directions with a positive gradient in proportion to the weighted slope. The total groundwater flow out of each cell is therefore the following function of the deficit state variable, D:

$$Q(D) = \frac{k_s.\Delta x}{f}.\sum_{k=1}^{8} \max[0,\ S_k.w_k].e^{-f.D/n} \qquad (3)$$

where S_k is the local ground slope in direction k, and w_k is a factor to account for the width of flow in each direction. When S_k is negative, the ground slopes toward the cell from the direction k, and the max[.] function in equation (3) excludes that flux from the outflow sum.

By combining (1) and (3), the deficit balance equation can be written as:

$$\Delta x^2 \frac{dD}{dt} = \frac{k_s.\Delta x}{f}.\sum_{k=1}^{8} \max[0,\ S_k.w_k].e^{-f.D/n} - \{I(t) + SF(t)\} \qquad (4)$$

This couples the deficit D at each cell with the deficit in adjacent cells through the inflow I(t), and to the surface mass and energy balances through SF(t). The assumption that subsurface gradients follow the topography means that a simultaneous solution of the mass balance equations is not required. Individual budgets are solved for upstream cells before downstream cells. When solving (4), I(t) and S(t) are known inputs, taken as constant for a time step and, therefore, it is an ordinary differential equation of the form:

$$\frac{dD}{dt} = C_1\, e^{-f\,D/n} - C_2 \qquad (5)$$

where C_1 and C_2 include all the constants in the terms on the right hand side of Equation (4).

Given an initial deficit D, equation (4) has an analytic solution which is used to obtain D at the end of the time step, and the outflow Q, which contributes to the inflow I for down-gradient cells. If a cell becomes saturated, D is set to zero, and input in excess of transmissivity is routed downstream as

surface runoff without reinfiltrating. Surface runoff will continue to be produced from the cell for all subsequent time steps in which D = 0 and I + SF > Q.

Infiltration capacity limitations and the lag due to infiltration through the unsaturated zone are neglected in the calculation of the SF component of cell inflow. Isotope data given by Unnikrishna (1995) confirm that much of the snowmelt at Upper Sheep Creek moves very quickly through unsaturated soil to depth, so snowmelt goes to reduce the deficit, D, almost immediately. This does not hold for rainfall on dry soil, however, which has implications for model accuracy that are discussed below.

2.4 Snow Fall Accumulation and Redistribution

Moisture enters the watershed system as precipitation. The total measured precipitation, P, is reported in terms of equivalent water depth. In the model, P is partitioned into rain, P_r, and snow, P_s, based on the air temperature, T_a. When the $T_a > 3\,^{\circ}C$, $P_r = P$; for $T_a < -1\,^{\circ}C$, $P_s = P$. For $-1\,^{\circ}C < T_a < 3\,^{\circ}C$, a mixture is assumed (U.S. Army Corps of Engineers, 1956):

$$P_s = P * \frac{3 - T_a}{4} \qquad (6)$$

Air temperature, measured at the gage, is adjusted for each cell using a lapse rate of 0.0065 °C/m, so the partitioning of precipitation within the catchment is dependent on the local elevation.

Snow fall at the study site is subject to significant redistribution due to wind, so that serious mass balance errors would result from applying recorded snow gage depths uniformly across the basin

(Cooley, 1988). Accounting for drift is one of the most serious obstacles to accurate distributed modeling of the snowmelt process (Bloschl et al, 1991; Obled and Harder, 1978). We accounted for this in the model through a snow drift factor, $F_{j,i}$, calculated for each cell by assuming that, over a time interval between measurements, the difference between observed SWE, Wo, and simulated SWE, Wm, was entirely due to drifting.

A snow budget for each DEM cell during the period between two snow surveys was written as:

$$Wo_1 + Drift_{1-2} + P_{1-2} + C_{1-2} - M_{1-2} - E_{1-2} = Wo_2 \qquad (7)$$

where Wo_1 and Wo_2 are the measured values at the start and finish of the period, and M_{1-2}, E_{1-2}, C_{1-2}, and P_{1-2} are cumulative fluxes of melt, evaporation, condensation, and precipitation on the snow during the period. $Drift_{1-2}$ was taken as the volume required for closure of the mass balance using simulated fluxes and observed precipitation and SWE, implicitly assuming that the snowmelt model correctly accounts for all other processes (melt, sublimation, condensation, etc.) affecting the accumulation and ablation of snow.

A positive value of drift indicated that snow in excess of precipitation was transported on to the cell and a negative value indicated transport off the cell.

The drift factor was calculated for each cell as:

$$F_{j,i} = 1 + \frac{Drift_{1-2}}{P_s} \qquad (8)$$

where P_s is the amount of measured precipitation estimated to be in the form of snow, based on air temperatures (equation 6). Values of $F_{j,i}$ greater than one correspond to locations of drift accumulation, while values of $F_{j,i}$ less than one correspond to locations of depletion or wind scour. This approach models drifting which actually occurs after snow fall as concurrent with snow fall, but that is not a significant source of error for surface melt quantities occurring many weeks after snow fall has occurred.

This method can produce a negative, and obviously erroneous, drift factor if the proportion of precipitation falling as snow is underestimated, or due to model errors such as the overestimate of ablation where snow depth is shallow or snow cover is intermittent. In the application below a small number of negative drift factors occurred on south facing slopes. An arbitrary value of 0.0001 was assigned to these cells.

2.5 Snow Melt

A two-state energy and mass balance model (Tarboton et al., 1995) was used to model the snow melt and ablation from the snow pack on each cell at each time step. The state variables are water equivalent, W[m], and energy content U [kJ/m^2], of snow and upper layer of soil, relative to a reference state at 0 °C. Evolution of the snow pack at a cell is modeled as

$$\frac{dW}{dt} = P - M_r - E \tag{9}$$

$$\frac{dU}{dt} = R_{net} + Q_p - H - l_s \rho_w E - l_f \rho_w M \tag{10}$$

where E is sublimation, M melt outflow, R_{net} radiation, Q_p heat advected by precipitation, H sensible heat flux, ρ_w the density of water, l_s the latent heat of sublimation and l_f is the latent heat of fusion.

Latent and sensible heat fluxes are modeled using a bulk aerodynamic approach dependent on wind speed and the vapor pressure (as determined from measured relative humidity) and temperature gradient between the air and snow surface. Net radiation comprises short and longwave radiation with albedo a function of snow surface age. Outgoing longwave radiation is modeled using the Stefan-Boltzman equation and snow surface temperature. Incoming longwave radiation is similarly calculated from air temperature and emissivity parameterized in terms of vapor pressure.

Energy balance modeling was simplified for this study because horizontal plane measurements of incident shortwave solar radiation were available on an hourly basis. This eliminated the need to account for the effect of cloudiness.

Heat advected by precipitation was calculated by taking the precipitation at air temperature or 0°C, as appropriate, for rain and snow. Melt outflow was calculated using Darcy's equation and gravity drainage through the snow with the liquid fraction determined from the energy content and water equivalent, and the hydraulic conductivity of the snow a function of relative saturation.

Following Kondo and Yamizaki (1990), this model expresses surface energy fluxes in terms of snow surface temperature, which is calculated using an equilibrium approach that balances the energy fluxes at the surface with conduction into the snow, driven by the difference between the snow surface temperature and the average temperature of the snow pack, as determined from U and W. This temperature difference is taken to act over the depth of penetration of diurnal temperature fluctuations.

This model was calibrated against data from the Central Sierra snow laboratory then tested against snow data collected at Upper Sheep Creek and an Experimental farm in Logan, Utah (Tarboton et al., 1995,

Tarboton 1994) performing satisfactorily in both cases. It was used here without further calibration except for the estimates of drift parameters as described in Section 4.1

2.6 Evapotranspiration

During time steps when there is no snow on the ground evapotranspiration (ET) occurred. In this work ET was calculated based on a combination of energy balance and resistance equations with inputs of standard meteorological data, including air temperature, relative humidity, wind speed, and solar radiation to estimate the vapor fluxes from each grid cell. Our approach was based on the Priestley-Taylor equations and soil moisture availability, recognizing that, in an arid environment, moisture availability is frequently a more important control over ET than energy and atmospheric transport limitations. Evapotranspiration was taken as the Priestley-Taylor potential evapotranspiration, reduced by a multiplier, α, which is a function of subsurface moisture deficit:

$$\lambda E = \alpha(\theta) \frac{\Delta}{\Delta + \gamma}(R_n - G) \tag{11}$$

$$\alpha(\theta) = \alpha(z_s) = \frac{1.26}{1 + \beta z_s} \tag{12}$$

where Δ is the slope of the saturation vapor pressure-temperature function, γ the psychometric constant, and λE the latent heat flux. The Priestley-Taylor factor $\alpha(\theta)$ is reduced below the nominal value of 1.26 as subsurface moisture deficit, z_s, increases, the rate of this reduction being controlled by the parameter β. A drawback of this approach is that it is really the near surface soil moisture that affects evaporation, while z_s characterizes the subsurface moisture deficit over its full depth.

Ground heat flux, G, evolving as dU/dt, is the flux from the surface into the same upper layer of

soil as used for the snowmelt model. This allows the calculation of the state variable U and the modeling of the storage of energy near the soil surface, providing continuity between periods with and without snow on the ground. The surface energy balance equation is written:

$$R_n = G + \lambda E + H \tag{13}$$

R_n, H and G all depend on surface skin temperature which is calculated to balance these fluxes. This approach accounts in a simple way for variations in surface temperature and its effect on evaporation, through R_n-G, and storage of energy in the top soil layer.

3.0 FIELD SITE

Upper Sheep Creek is a 26 ha catchment within the semi-arid Reynolds Creek Experimental Watershed in southwest Idaho. Vegetation is primarily sagebrush with localized stands of aspen on north facing slopes. Detailed descriptions of the various features of the area are given in Stephenson and Freeze (1974) and Flerchinger et al. (1992). Snowmelt is the main hydrologic input and its areal distribution is heavily influenced by wind induced drifting.

The evaluation of the model at this site was facilitated by the availability of basin-wide distributed data, in particular, measurements of SWE on a 30.48 m (100 ft) grid. A 255-cell DEM was constructed from a 1:1200 map with 0.61 m (2 ft) contour intervals developed from low level aerial photography to coincide with the grid used for field measurements. Figure 2 shows the topography and grid over Upper Sheep Creek, locations of the instrumentation used, and soil type boundaries estimated from Stephenson (1977).

3.1 Site Climate Data

Hourly data from the winters of 1985/86, water year 1986 (WY86) and 1992/93 (WY93) were used in this study. This data included:

1) Average Air Temperature, degrees Centigrade.

2) Wind Run and Direction, miles & degrees respectively.

3) Horizontal Incident Solar Radiation, W/m^2.

4) Precipitation measured using the dual shielded and unshielded gage system (Hanson et al., 1979).

5) Relative Humidity, in percent.

3.2 Stream flow data

The ARS measures runoff from Upper Sheep Creek with a V-notch weir installed in the main channel. Stream flow is ephemeral and occurs mainly in the months of May and June. Reynolds creek experienced a drought from 1986 to 1992; essentially no runoff was recorded at Upper Sheep Creek during the included winter seasons.

3.3 ARS Snow Surveys

The spatial and temporal variation in the snow pack at Upper Sheep Creek has been studied extensively, using data obtained from aerial photography and a 300-point snow course. Based on observations from 1984 through 1987, Cooley (1988) reported an annually recurring pattern of snowmelt and ablation:

1) Intermittent snow cover on the upper portion of the south facing slopes and ridges due to favorable aspect with respect to the winter sun and exposure to southwesterly winds.

2) General snow cover in the central portion of the watershed where the exposure to wind and radiation is less.

3) Drift areas on the lee sides of the ridges. These drifts persist into early summer and constitute a major source of moisture for peak runoff. These drifts are also associated with stands of aspen which depend on the moisture they provide.

The SWE maps from the snow surveys are shown for the 1986 and 1993 spring melt seasons in figures 5a and b. These figures show similar topographically controlled patterns of snow accumulation and melt each year. The large wind blown drifts that form behind the ridges are evident.

Melt collectors were installed by the ARS to measure the point melt rate in snow columns at three locations in the basin (see figure 2). The collectors are metal cylinders, buried with the rim about 25 mm above ground level to prevent the lateral inflow of extra melt water. Meltwater from the overlying snow column is conducted from the cylinders to a tipping-bucket mechanism for measurement (Flerchinger et al., 1992).

Cumulative melt data for the two collectors identified as "D3" and "L10" are plotted in figure 6 for the 1985-6 snow melt season. Melt collector D3, on the south facing slope, is representative of the response of the intermittent melt zone; site L10 is representative of the drift area.

The cumulative melt curves confirm the timing and pattern of snow melt reported by Cooley (1988). The general melt on the south slope occurs earlier in the season than the melt in the drift area. By the date of the first snow survey on February 25 (or day 421), much of the general snow cover has already melted.

4.0 MODEL APPLICATION AT UPPER SHEEP CREEK

While all watershed processes are integrated and operate simultaneously, we divided the model into two main components:

1) the *surface* energy and mass balances for the determination of evapotranspiration and the surface water input of rainfall and snowmelt,

2) the *subsurface* model for the determination of spatially variable moisture storage and outflow from the basin.

Following Blöschl, Kirnbauer and Gutnecht (1991), the surface snowmelt model was calibrated independently of the subsurface model. Drift was accounted for in the accumulation of snow in the watershed and melt rates determined from the adjusted surface model were used as input to the subsurface model.

We calibrated our model with data from the 1985-6 water year and used comparisons of simulated and observed response in the 1992-3 melt season to validate the model.

4.1 Surface water input calibration

The snowdrifts evident in figure 5 indicate the importance of accounting for snow drift accumulation to correctly model the surface water inputs. In WY86, grid SWE measurements were available on the six dates indicated in figure 5a. The model was initialized on 10/29/85 before any snow fell. Most of the snow accumulation and drifting occurred prior to 3/26/86, so the average drift factor for the first two periods 10/29/85-2/25/86 and 2/25/86-3/26/86, weighted by the period length in days, was calculated.

A map of these weighted average drift factors is shown in figure 7. The areal distribution of the weighted average drift factors is consistent with the pattern of prevailing south-westerly winds at the site. The area with factors less than 0.25 coincides with the windward slopes and ridges, and factors greater than 1 correspond with areas in the lee of the north-facing slope.

These drift factors were used to run the model for the calibration year, WY86, and the verification year, WY93. Drift corrections were applied up to 3/26 in each year, after which no corrections were applied to measured precipitation.

Simulated and measured point melt quantities at cells D3 and L10 are shown in figure 6. After the general melt, simulated heat exchange at the snow surface did not supply sufficient energy to melt the drift as quickly as was observed, as shown by the lag of the simulated melt behind the observed melt at site L10, in figure 6. Figure 8 shows the observed and simulated SWE in the Upper Sheep Creek watershed on 3/3/93, 4/8/93 and 5/19/93 (in the verification year). An inspection of the figures indicates that the application of the point energy balance snow melt model on a distributed basis simulated the disappearance of the "general melt" as described by Cooley (1988) reasonably well, so that only the drift area retained snow cover in the late season.

Since overland flow was not observed below the drifts at Upper Sheep Creek during this study or in prior work (Flerchinger et al., 1992), all snow melt and all precipitation on bare ground was assumed to infiltrate into the cell on which it occurred. Based on this assumption, figure 9 shows contour maps of the total simulated infiltration of meltwater up to the first snow survey, on February 25, and at the end of the 1985-86 snowmelt season in July.

An inspection of figure 9 shows that, except for the windward and NE ridge areas, all parts of the watershed receive at least 25 cm of annual infiltration. Annual infiltration in the drift area is an order

of magnitude larger. This pattern of moisture infiltration has a profound influence on soil structure in the watershed, as can be seen from the coincidence of the drift areas shown in the figure and the boundaries of permeable soil shown in figure 2.

4.2 Subsurface model calibration

Rainfall and snowmelt output from the surface model becomes input to the subsurface model. The subsurface component of the model simulates the lumped moisture deficit, D, of each cell by a solution of the water budget differential equation presented in Section 2.2.

A moisture deficit must be specified as an initial condition, which is analogous to the selection of an antecedent moisture condition (AMC) for event-based models. The calculation of these initial deficits were based on an initial base flow, Q_w. Following the topography-driven model approach (Beven and Kirkby, 1979; O'Loughlin, 1986), we assumed that each cell contributes to basin outflow in proportion to the ratio of its contributing upslope area, a_i, and the basin area, A. This flow was substituted in equation (3) to get the initial deficit, D_o, for each cell:

$$D_o = -\frac{n}{f} \ln \left(\frac{a.f.Q_w}{A.k_s.\Delta x.\sum_{k=1}^{8} \max[0, S_k.\omega_k]} \right) \qquad \textbf{(14)}$$

Calculating initial conditions of moisture storage in the watershed with equation 14 requires a non-zero Q_w. Since the ARS reports no flow over the outlet weir at Upper Sheep Creek after the end of the runoff season, Q_w should be considered as an index of antecedent moisture conditions (AMC) for this catchment rather than an exactly quantifiable flux. Higher values of Q_w indicate more humid antecedent conditions; a lower value of Q_w results in a larger initial deficit and a reduced total volume of runoff.

The overall runoff response is sensitive to the parameters k_s and f, as well as the initial conditions indexed by Q_w. To reduce the degrees of freedom in the calibration against 1985/86 data we held Q_w fixed at 0.01 m^3/hr.

Calibration of k_s and f was carried out in two stages. First, basin-wide uniform values of k_s and f were chosen within the range reported in the literature to obtain a match between the simulated and observed total season runoff (estimated from ARS measurements as an area average of 95.5 mm for WY86).

In the second stage of calibration, spatial variability was explicitly accounted for. Starting with the best first-stage values of f and k_s, f was varied systematically for each soil zone to minimize the discrepancy between the timing and magnitude of peak runoff at the daily and weekly time scales for the observed and simulated hydrographs. The details of both phases of the calibration procedure are presented in the following two sections.

4.2.1 First stage calibration: uniform k_s and f values

A homogeneous soil with uniform values of k_s and f across the site was assumed in the first stage of calibration.

The model was run with two different values of the basin-wide effective hydraulic conductivity to test the effect of the parameter on the simulated extent of variable saturated area. The values used were 0.6 m/hr and 3.0 m/hr, which are consistent with the median and upper range of the estimates of hydraulic conductivity for permeable basalt formations (Freeze and Cherry, 1979).

Figure 10 shows the sensitivity of total initial moisture deficit (estimated from equation 14) and total season outflow obtained by varying the uniform basin f-value for the two selected values of the

basin-wide k_s. Equation (14) shows that as f is increased the initial deficit decreases for Q_w and k_s constant. This decrease in initial deficit results in an increase in the total season runoff volume. For the smaller of the two k_s values used, initial deficit is less and total season runoff more. In other words, a higher basin-wide f-value is required to obtain a given total basin runoff for k_s = 3.0 m/hr than for k_s = 0.6 m/hr.

Both sets of parameters (k_s = 0.6 m/hr, f = 4.26 m^{-1}) and (k_s = 3 m/hr, f = 4.75 m^{-1}) are acceptable in terms of matching overall runoff volume. However, with the first set about 18% of the watershed is surface saturated during peak snowmelt. For the second set this reduced to 6%. Since observations have indicated that apart from the channel itself, there are no significant areas of saturated soil in Upper Sheep Creek, the basin-wide parameters used were k_s = 3 m/hr and f = 4.75 m/hr.

Figure 11 shows the cumulative and daily average flow hydrographs obtained with these parameters, together with the observed data. The simulation successfully reproduces the total volume of runoff and the timing of the initial responses and peak flows, but the magnitude of peak flows is overestimated.

4.2.2 Second stage calibration: spatially variable f

The next step in calibrating the subsurface model was to account for the areal variation of subsurface conditions based on information obtained from the map of USDA soil types (see figure 2). Calibration consisted of varying the f-values assigned uniformly to each soil zone above or below the values obtained from the uniform calibration described above.

Equation (3) indicates the outflow response from each cell. Assuming the catchment as a whole responds in a qualitatively similar manner, total catchment discharge, Q varies as:

$$Q \sim \frac{k_s}{f} e^{-f D/n} \quad (15)$$

The parameter f controls the sensitivity of cell and watershed outflow to changes in storage. By increasing f, smaller changes in storage, D, are required to affect a given change in runoff. Therefore, f can be used to tune the response of individual DEM cells. This tuning was accomplished by inspecting the hydrograph and maps of surface snowmelt input to match components of the hydrograph with the spatial location of the corresponding melt input. While keeping k_s fixed ($k_s = 3$ m/hr), we adjusted f values in soil type zones (see figure 2) to reduce the differences between the simulated and observed hydrograph. The overestimated peak runoff at day 520, for instance, as seen in figure 11, was reduced by a decrease of f-values in soil zones HbF and GfG. The set of f values we obtained in this process was 4.75, 5.15, 5.15, 2.9, and 2.7 m^{-1} in soil type zones GaG, HmG, GfF, HbF, and Gfg, respectively. Figure 12 shows the best fit to the observed runoff hydrograph obtained by the calibration process described above.

4.3 Evaluation of the 1985-6 Budget

Figure 12 also presents climate inputs (precipitation and temperature), and snow storage components plotted on the same time scale. This shows that the model integrates the effects of the processes operating in and on the basin to provide reasonable estimates of snow storage and watershed yield over time.

Figure 13 shows the cumulative basin-wide surface and subsurface water balance. The set of curves in the upper half of the figure represents cumulative fluxes at the surface of the basin which can be written as:

$$Sublimation + Melt + SnowVol. = Precipitation + Condensation \quad (16)$$

so that the vertical distance between any two points on the lines representing total cumulative input to, and total efflux from, the snow pack is a volume of snow in storage in figure 13. For comparison, the volumes of snow calculated from the ARS snow surveys at the site during the season are plotted on the curve at the appropriate date. The lone trace separating the upper and lower groups of lines (third from the bottom) represents the cumulative melt from the snow pack, which is also the infiltration input to the subsurface model. The two lower lines in the graph represent cumulative subsurface fluxes out of the basin: drainage at the outlet weir, where all subsurface drainage is included as runoff, and the depletion of soil moisture by evapotranspiration. The cumulative observed runoff is also shown for comparison. The vertical distance between the inflow and the combined runoff and ET outflow is soil moisture storage at a given time.

The total season simulation extended from October 29 to September 30. In this period, infiltration of rain and snow-melt amounted to a basin average depth of 534 mm, as shown in table 2. Some 40 percent of this volume (219 mm) was removed from the soil by evapotranspiration, 20 percent (107 mm) left the basin as surface runoff, and the remainder (208 mm) went to reducing the watershed subsurface moisture deficit (i.e., it was added to "soil moisture" storage).

The partitioning of moisture between the different stores and fluxes is affected by the f-values assigned to each cell, but there is no differentiation between soil moisture storage and deep percolation. The f-values for each zone account for storage in terms of transmissivity, so that the 208 mm reduction in basin average moisture deficit is really a *detention* storage — moisture that does not leave the basin during the simulation.

On the average, there should be no change in deficit (or storage) over a year. Figure 13 indicates that this condition was not met for the 11-month period simulated. The initial and final moisture deficits

differed by 208 mm, or about 35 percent, which would have been less, given another month of active ET.

The total simulated actual ET for the period was a basin-wide average depth of 219 mm. The simulated PET for the period was 319 mm. National weather service charts (Bras, 1990) indicate an annual PET for this region of 950 mm. Therefore, both AET and PET appear to be underestimated. Low ET fluxes could be a significant source of error in the annual water budget; increased values would reduce the quantity of water attributed to interannual storage. If ET *is* underestimated, then a simulation with upward-adjusted ET would more closely approximate the condition of no net change in storage.

Also, since 1985-6 was a "wetter than average" season at Upper Sheep Creek, and the 1984-5 season was "dryer than average," it might be expected that storage would be replenished to some extent, and the year-end deficit would not return to the value at the beginning of the year.

4.4 Test Against 1992-3 Season

To provide verification of the model, the 1992-3 snowmelt season was simulated using the parameters calibrated from the 1985-6 season, including that season's average drift factors applied for the same period. Q_w was reduced from 0.01 to 0.00375 m^3/hr, to match the observed runoff volumes in the early snowmelt season. This reflects the drier antecedent moisture conditions reported for 1992.

Observed and simulated maps of SWE for the 1992-3 season were shown in figure 8. These indicate that the snowmelt model reasonably reproduces the overall spatial patterns of snow accumulation and ablation. However, the total snow volumes are larger than observed, as shown in figure 14. This results in too much surface water input and an overestimated streamflow hydrograph. To evaluate the performance of the model for the rest of the season, we ran the model until March 3, 1993, and then reinitialized the SWEs for each cell with the observed peak snow accumulation. Figure 15 shows the climatic inputs, SWE

comparisons, and observed and simulated daily average runoff hydrograph for the 1992-3 season at Upper Sheep Creek before and after the March 3 reinitialization. Inspection of the figure indicates that the modeled ablation of snow closely follows the observed pattern for the rest of the melt season.

Table 2, referred to in section 4.3, also gives the basin-wide water budget components predicted by the model for the 1992-3 season. By the date of reinitialization, a basin average of 269 mm of snow had accumulated; 280 mm of additional precipitation and 17 mm of condensation less 42 mm of sublimation make up the total 524 mm of surface moisture infiltration for the water year. This was partitioned by the model into 115 mm of surface runoff and 177 mm of soil moisture ET, with 232 mm going into subsurface storage. The difference between the initial and final subsurface deficit is high, but reflects the fact that our runs ended on 8/16/93 while ET was still a fairly active process. Also, it is very possible that there is appreciable cross year storage in this small catchment.

Figure 16 is a plot of the simulated cumulative surface and subsurface water budgets for the 1992-3 snowmelt season at Upper Sheep Creek. A comparison with the similar plot for the 1985-6 season in figure 13 shows that most of the differences between the basin response in the two seasons is caused by the timing of snowfall and the rate of its ablation.

The overall shape of the catchment outflow hydrograph to day 525 is fairly well modeled although somewhat spiky. The timing of the peak runoff at day 500 is correctly simulated. A runoff spike is modeled at day 525 as the response to a 40-mm rainstorm event, but ARS streamflow records at the outlet weir show minimal streamflow response in response to this event. This indicates that the model adequately simulates snowmelt runoff, but does not represent the lack of runoff response due to large rainfall on dry soil. This is because we did not model soil moisture storage in the unsaturated zone. A quantitative change in soil moisture storage after the snowmelt season leads to a qualitative change in basin response.

Under snow melt conditions, the unsaturated zone simply transmits water vertically downward to the saturated zone. Extractions due to evapotranspiration are minimal. However, after the snow has ablated, evapotranspiration depletes unsaturated zone soil moisture below field capacity. The 40 mm of rain appears to have been absorbed by this dry soil resulting in the negligible runoff response.

5.0 CONCLUSIONS

The simple DEM-based mass balance model we developed for Upper Sheep Creek successfully simulated the effects of topography on energy and mass balances at the hillslope scale in a small arid mountain catchment. The seasonal changes in the areal distribution of moisture within the catchment, and the timing and magnitude of the early melt season hydrographs were successfully reproduced for the verification year. Errors in the simulation of late season runoff response were due to simplifying assumptions that can be readily accounted for in future versions of the model.

Specific observations and conclusions concerning the model and the hydrologic response of small arid mountain catchments coming out of our study are:

1) It is essential to account for the effect of snow drifting. A dynamic drift model requires distributed values of wind speed and direction. However, the pattern of drifting was adequately estimated from snow surveys. Drift factors estimated this way for one year were successfully applied in another year to obtain the basic distributed pattern of accumulation and ablation, although total peak snow accumulation was overestimated by about 25 percent for the test year.

2) The point energy balance applied to each DEM cell in the model correctly responded to local topographic attributes such as slope and aspect. Simulated melt rates corresponded with observed rates

on the north and south-facing slopes after drift factors were applied. The masking of melt model errors with drift factors appeared to be minimal.

3) It is apparent that the spatial and temporal variation of surface snowmelt inputs has a very strong effect on the hydrologic response of Upper Sheep Creek. This was used to advantage in the calibration of the model. Because the time of concentration is small compared to the length of the periods between surveys, it was possible to separate the hydrograph into components originating from specific snowmelt zones. Adjusting the value of f for cells in these zones provided a physically meaningful method of calibration.

4) The lack of an unsaturated storage and vertical flux component simplified the model but made the runoff response spiky. Evidently one of the effects of an unsaturated zone is smoothing of surface water inputs. The absence of an unsaturated storage component also resulted in errors in modeling the response of the watershed to rainfall on dry soil. This will be one of the issues that future work will address.

Overall, we feel that this work has lead to a better understanding of the water balance at Upper Sheep Creek and has demonstrated the potential for successfully applying DEM-based distributed models to the study of other mountain catchments. The combination of modeling and data analysis we employed helped us to identify problems in some of the details of our modeling approach that will be addressed in future studies on the Reynolds Creek area.

6.0 ACKNOWLEDGMENTS

This work was funded in part by the United States Geological Survey, Department of the Interior, under USGS Grant No. 14-08-0001-G2110. The views and conclusions are those of the authors and should not be interpreted as necessarily representing the official policies, either expressed or implied, of the U.S. Government.

We would also like to thank Roland P. Jeppson and Upmanu Lull, of Utah State University, and Gerald Flerchinger of the Agricultural Research Service for their reviews of the first draft of this manuscript.

7.0 REFERENCES

Band, L.E. 1986. Topographic partition of watersheds with digital elevation models. Water Resources Research 22(1):15-24.

Band, L.E. and E.F. Wood. 1988. Strategies for large-scale distributed simulation. Applied Mathematics and Computation 27:23-27.

Beven, K.J. and M.J. Kirkby. 1979. A physically based, variable contributing area model of basin hydrology. Hydrological Sciences Bulletin 24(1):3-17.

Beven, K. and E.F. Wood. 1983. Catchment geomorphology and the dynamics of runoff contributing areas. Journal of Hydrology 65:139-158.

Beven, K., (Ed.) 1992. The future of distributed hydrologic modeling. Hydrologic Processes 6(3):253.

Beven, K. and A. Binley, 1992. The future of distributed hydrologic modeling: model calibration and uncertainty prediction. Hydrologic Processes, 6:279-298.

Bloschl, G., R. Kirnbauer, and D. Gutnecht. 1991. Distributed snowmelt simulations in an alpine catchment. 1. Model evaluation on the basis of snow cover patterns. Water Resources Research 27(12):3171-3179.

Bras, R.L. 1990. Hydrology. An introduction to hydrologic science. Addison-Wesley Publishing Company, New York. 643 p.

Chorley, R.J. 1978. The hillslope hydrologic cycle, Chapter 1. in M.J. Kirkby (Ed) Hillslope Hydrology. John Wiley and Sons, New York. 389 p.

Cooley, K.R., 1988. Snowpack variability on western rangelands. In Proceedings, Western Snow Conference, Kalispell, Montana, April 18-20.

Flerchinger, G.N., K.R. Cooley, and D.R. Ralston. 1992. Groundwater response to snowmelt in a mountainous watershed. Journal of Hydrology 133:293-311.

Freeze, R.A. and J.A. Cherry. 1979. Groundwater. Prentice-Hall, Englewood Cliffs, New Jersey. 604 p.

Grayson, R.B., I.D. Moore and T.A. McMahon, 1992a. Physically based hydrologic modeling 1. A terrain-based model for investigative purposes. Water Resources Research, 28(10):2639-2658.

Grayson, R.B., I.D. Moore and T.A. McMahon, 1992a. Physically based hydrologic modeling 2. Is the concept realistic? Water Resources Research, 28(10):2659-2666.

Hanson, C. L., R. P. Morris and D. L. Coon, (1979), "A Note on the Dual-Gage and Wyoming Shield Precipitation Measurement Systems," Water Resources Research, 15(4): 956-960.

Jackson, T.H.R. 1994. A spatially distributed snowmelt-driven hydrologic model applied to Upper Sheep Creek. PhD Thesis. Utah State University.

Jenson, S.K. and J.O. Dominigue, 1988. Extracting topographic structure from digital elevation data for geographic information system analysis. Photogrammetric Engineering and Remote Sensing, 54(11):1593-1600.

Kirkby, M. 1986. A runoff simulation model based on hillslope topography, Chapter 3. in V.K. Gupta, I. Rodriguez-Iturbe, and E.F. Wood (Eds.). Scale Problems in Hydrology. Kluwer Academic Publishers, Boston, MA. 246. p.

Kondo, J. and T. Yamazaki. 1990. A prediction model for snow-melt, snow surface temperature and freezing depth using a heat balance method. Journal of Applied Meteorology 29:375-384.

Moore, I.D. (Ed.) 1991. Special Issue: Digital terrain modeling in hydrology. Hydrologic Processes 5(1).

Moore, I.D. and R.B. Grayson. 1991. Terrain-based prediction of runoff with vector elevation data. Water Resources Research 27(6):1177-1191.

Moore, I.D., R.B. Grayson, and A.R. Ladson. 1991. Digital terrain modeling: a review of hydrological, geomorphological. and biological applications. Hydrologic Processes 5:3-30.

Obled, C. and H. Harder, 1978. A review of snowmelt in the mountain environment. In S.C. Colbeck and M. Ray (Eds.), Proceedings Modeling of snow cover runoff, U.S. Army Cold Regions Research and Engineering Laboratory, Hanover, NH, September 26-28, pp 179-204.

O'Callaghan, J.F. and D.M. Mark, 1984. The extraction of drainage networks from digital elevation data. Computer Vision, Graphics and Imaging Processing, 28:328-344.

O'Loughlin, E.M. 1981. Saturation regions in catchments and their relations to soil and topographic properties. Journal of Hydrology 53:229-246.

O'Loughlin, E.M. 1986. Prediction of surface saturation zones in natural catchments by topographic analysis. Water Resources Research 22(5):794-804.

Paniconi, C. and E.F. Wood. 1993. A detailed model for simulation of catchment scale subsurface hydrologic processes. Water Resources Research 29(6):1601-1620.

Quinn, P., K. Beven, P. Chevallier and O. Planchon. 1991. The prediction of hillslope flow paths for distributed hydrologic modeling using digital terrain models. Hydrologic Processes, 5:59-80.

Quinn, P.F., K.J. Beven and R. Lamb. 1995. The ln(a/tanβ)Index: how to calculate it and how to use it within the Topmodel Framework. Hydrologic Processes, 9:161-182.

Stephenson, G.R. and R.A. Freeze. 1974. Mathematical simulation of subsurface flow contributions to snowmelt runoff, Reynolds Creek Watershed, Idaho. Water Resources Research 10(2):284-294.

Stephenson, G.R. (Ed.). 1977. Soil-geology-vegetation inventories for Reynolds Creek watershed. Agricultural Experiment Station, University of Idaho College of Agriculture in Cooperation with Agricultural Research Service and Soil Conservation Service, USDA.

Tarboton, D.G. 1994. Measurement and modeling of snow energy balance and sublimation from snow. In Proceedings, International Snow Science Workshop, Snowbird, Utah, October 31 to November 2, Utah Water Research Laboratory working paper no. WP-94-HWR-DGT/002.

Tarboton, D.G., T.G.Chowdhury and T.H. Jackson, 1995. A spatially distributed energy balance snowmelt model. In K.A. Tonneson, M.W. Williams and M. Tranter (Eds.), Biogeochemistry of seasonally snow-covered catchments, Proceedings of a Boulder Symposium, July 3-14, IAHS Publ. No. 228, pp.141-155.

Troch, P.A., M.Mancini, C. Paniconi, and E.F. Wood. 1993. Evaluation of a distributed catchment scale water balance model. Water Resources Research 29(6):1805-1817.

Troendle, C.A. 1985. Variable source area models, chapter 12. In Anderson and Burt (Eds.) Hydrologic Forecasting. John Wiley and Sons, New York.

Unnikrishna, P.V. 1995. Stable Isotope Tracer Study of Flow Generation Mechanisms in a Small Semi-Arid Mountain Watershed. PhD Thesis. Civil and Environmental Engineering, Utah State University.

U.S. Army Corps of Engineers, 1956. Snow Hydrology, Summary Report of the Snow Investigations, USACE. North Pacific Division. Portland, Oregon.

Wigmosta, M. S., L. W. Vail and D. P. Lettenmaier, (1994), "A Distributed Hydrology-Vegetation Model for Complex Terrain," Water Resources Research, 30(6): 1665-1679.

Wolock, D.M. and G.J. McCabe, 1995. Comparison of single and multiple flow direction algorithms for computing topographic parameters. Water Resources Research, 31(5):1315-1324.

Wood, E.F., M.Sivapalan, K. Beven and L.Band. 1988. Effects of spatial variability and scale with implications to hydrologic modeling. Journal of Hydrology 102:29-47.

Table 1. Constituent components of energy and mass balances for each cell of the spatially distributed hydrologic model

FLUX MODELING (TRANSFERS)		
	VERTICAL:	HORIZONTAL:
Energy:	• Heat fluxes for snowmelt and ET	---
Mass:	• Precipitation	• Topography-driven subsurface flow
	• Evapotranspiration from soil	• Surface runoff
	• Snow Sublimation/Condensation	
	• infiltration from rain and snowmelt	
STORAGE MODELING (STATE VARIABLES)		
Energy:	• Energy content of soil/snow block, U	
	• Albedo of the plant/soil/snow block, A	
Mass:	• Snow Water Equivalent of Snow pack, W	
	• Soil Water Moisture Deficit, D	

Table 2. Mass balances for calibration and verification years of study (Entries are basin-wide average depths in mm).[1]

Start Date:	10/29/85	03/03/93[2]
End Date:	09/30/86	08/16/93
SURFACE SNOW PACK MOISTURE BUDGET		
Initial Snow depth	0	269
Total Precipitation depth	578	280
Total Snowfall depth	399	68
Sublimation	62	42
Condensation	18	17
Surface Water Input	534	524
SUBSURFACE SOIL MOISTURE BUDGET		
Initial Deficit	600	605
Infiltration	534	524
Soil Moisture Modeled ET	219	177
Potential ET	319	250
Basin Outflow	107	115
Period End Deficit	392	373

1) These are model results with soil zone-based f values (4.75,5.15,5.15,2.9,2.7)

2) WY93 water balance initialized at peak season snow accumulation SWEs

Figure 1. Reynolds Creek Experimental Watershed location map.

Figure 2. Upper Sheep Creek topography, instrumentation and soils (GaG, Gabica cobbly gravelly loam; HmG, Harmehl and Demast stony loam; GfF, Gabica very stony loam; HbF, Harmehl gravelly loam; GfG, Gabica very stony loam).

Figure 3. Definition sketch for DEM watershed modeling terms.

Figure 4. Schematic diagram for cell mass balance terms.

Figure 5a. 1986 observed snow water equivalence maps. 0.5 m contour interval.

Figure 5b. 1993 observed snow water equivalence maps. 0.5 m contour interval.

Figure 6. 1985-6 season cumulative snowmelt measured and simulated at sites D3 and L10.

Figure 7. Weighted average drift factors. Contours at 0.5, 0.9, 1.5, 2.5, 4, and 6.

Figure 8. Observed and simulated snow water equivalence maps.

Figure 9. Total simulated surface water input (rain + snowmelt) a) October 29, 1985 to February 25, 1986 and b) October 29, 1985 to July 4, 1986. Contours in m.

Figure 10. Initial deficit and total season runoff for a homogeneous catchment as a function of k_s and f.

Figure 11. Cumulative and daily average outflow hydrographs for the 1985-6 snow season at Upper Sheep Creek with uniform parameters.

Figure 12. 1985-6 hydrographs and climate inputs for final parameter set. Parameters are $k_s = 3$ m/hr and f = 4.75, 5.15, 5.15, 2.9 and 2.7 for soil types GaG, HmG, GfF, HbF, and GfG respectively.

Figure 13. Cumulative overall mass balance 1985-6.

Figure 14. Area average snow water equivalence.

Figure 15. 1992-3 hydrograph and climate inputs. Parameters are as for figure 13, 1985-6 data.

Figure 16. Cumulative overall mass balance 1992-3.

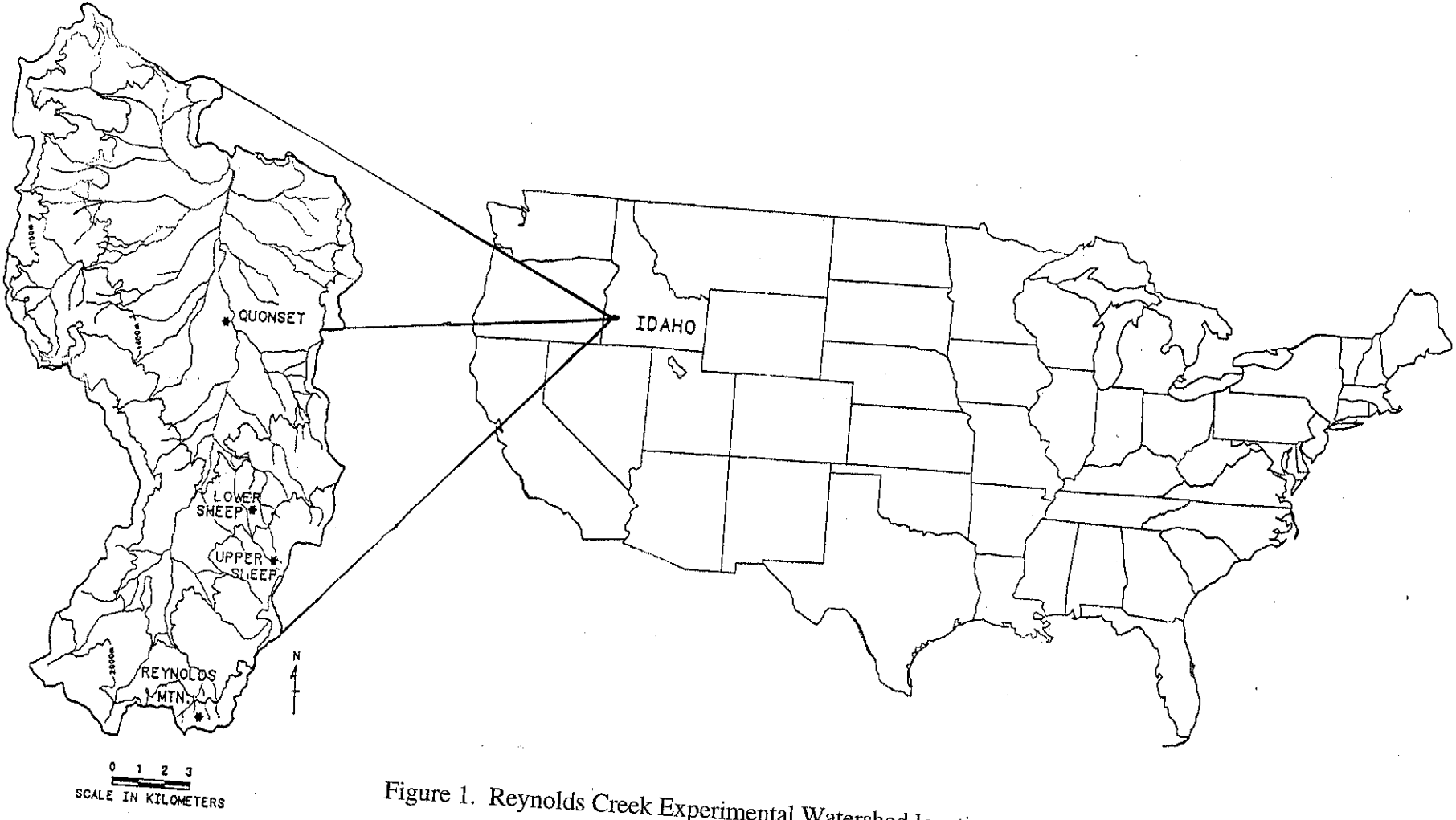

Figure 1. Reynolds Creek Experimental Watershed location map.

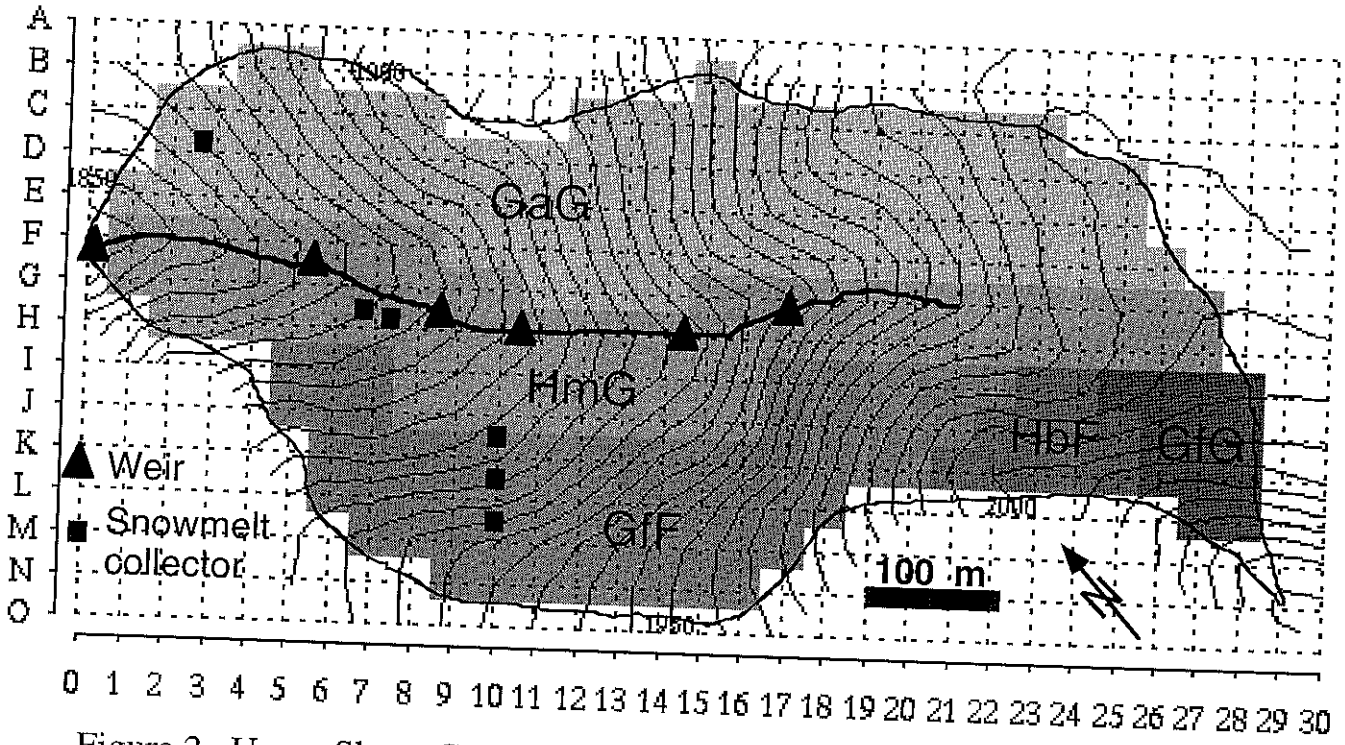

Figure 2. Upper Sheep Creek topography, instrumentation and soils (GaG, Gabica cobbly gravelly loam; HmG, Harmehl and Demast stony loam; GfF, Gabica very stony loam; HbF, Harmehl gravelly loam; GfG, Gabica very stony loam)

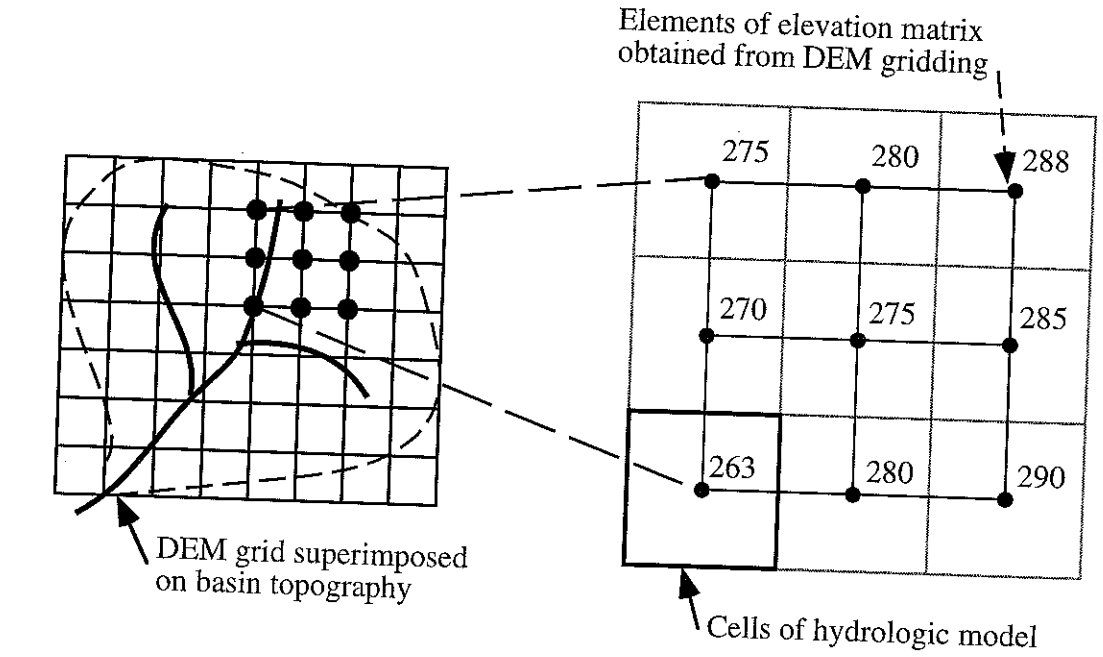

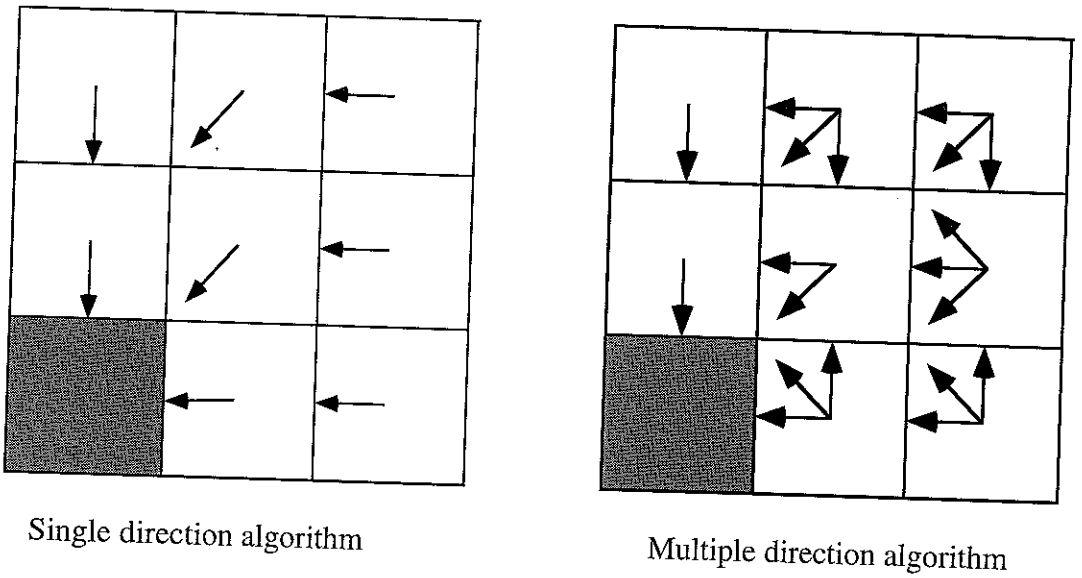

Figure 3. Definition sketch for DEM watershed modeling terms

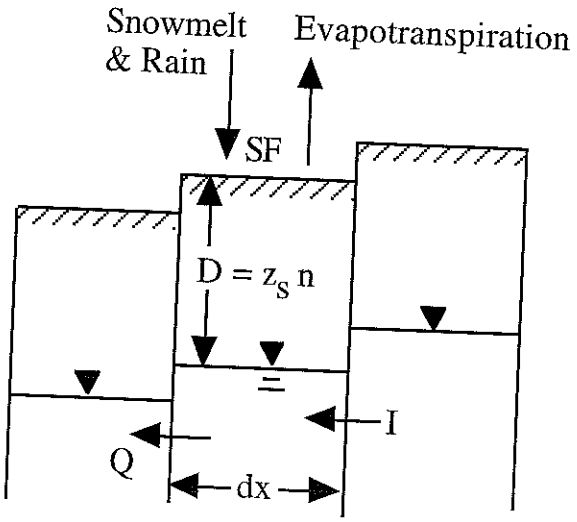

Figure 4. Schemtaic diagram for cell mass balance terms

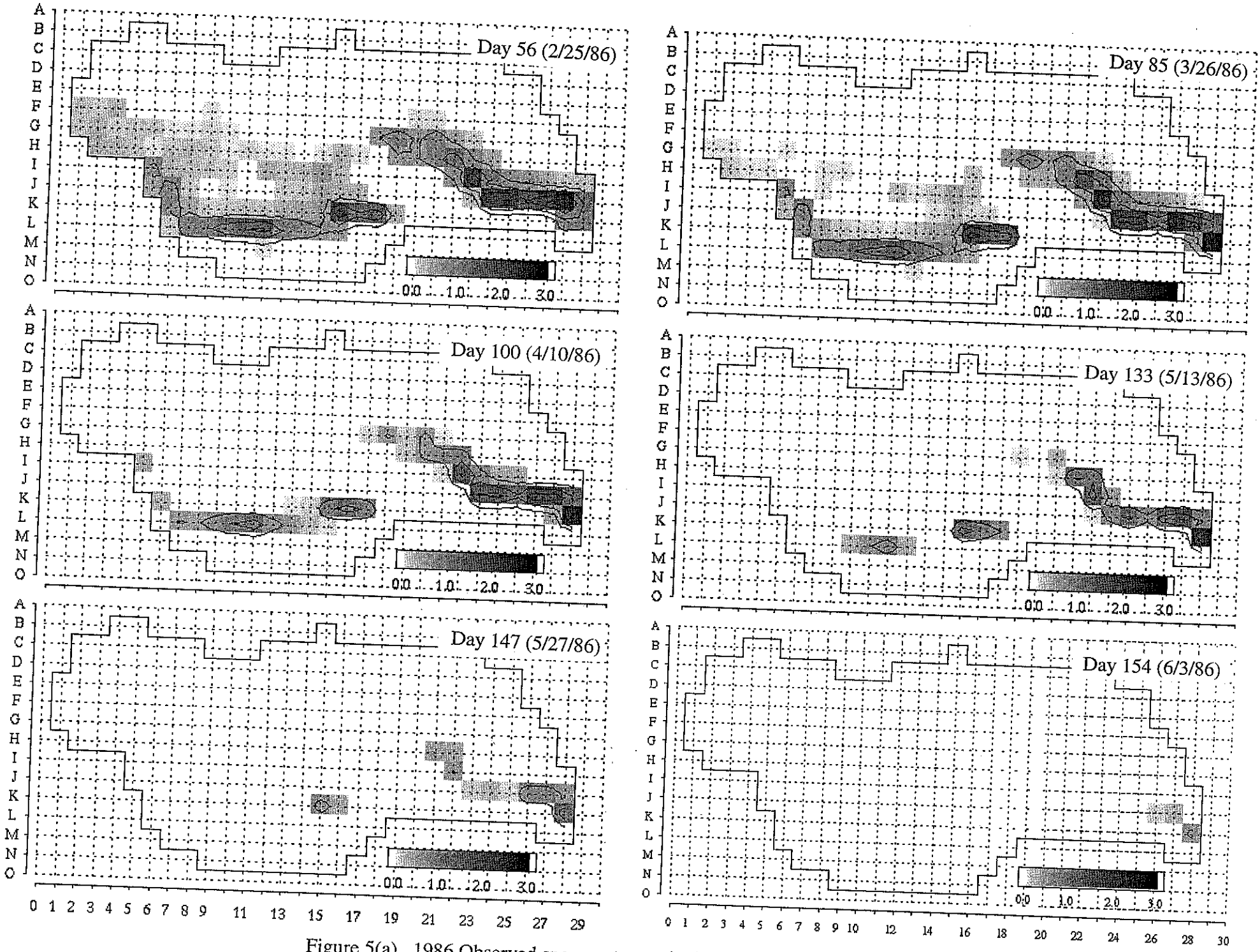

Figure 5(a). 1986 Observed snow water equivalence maps. 0.5 m contour interval.

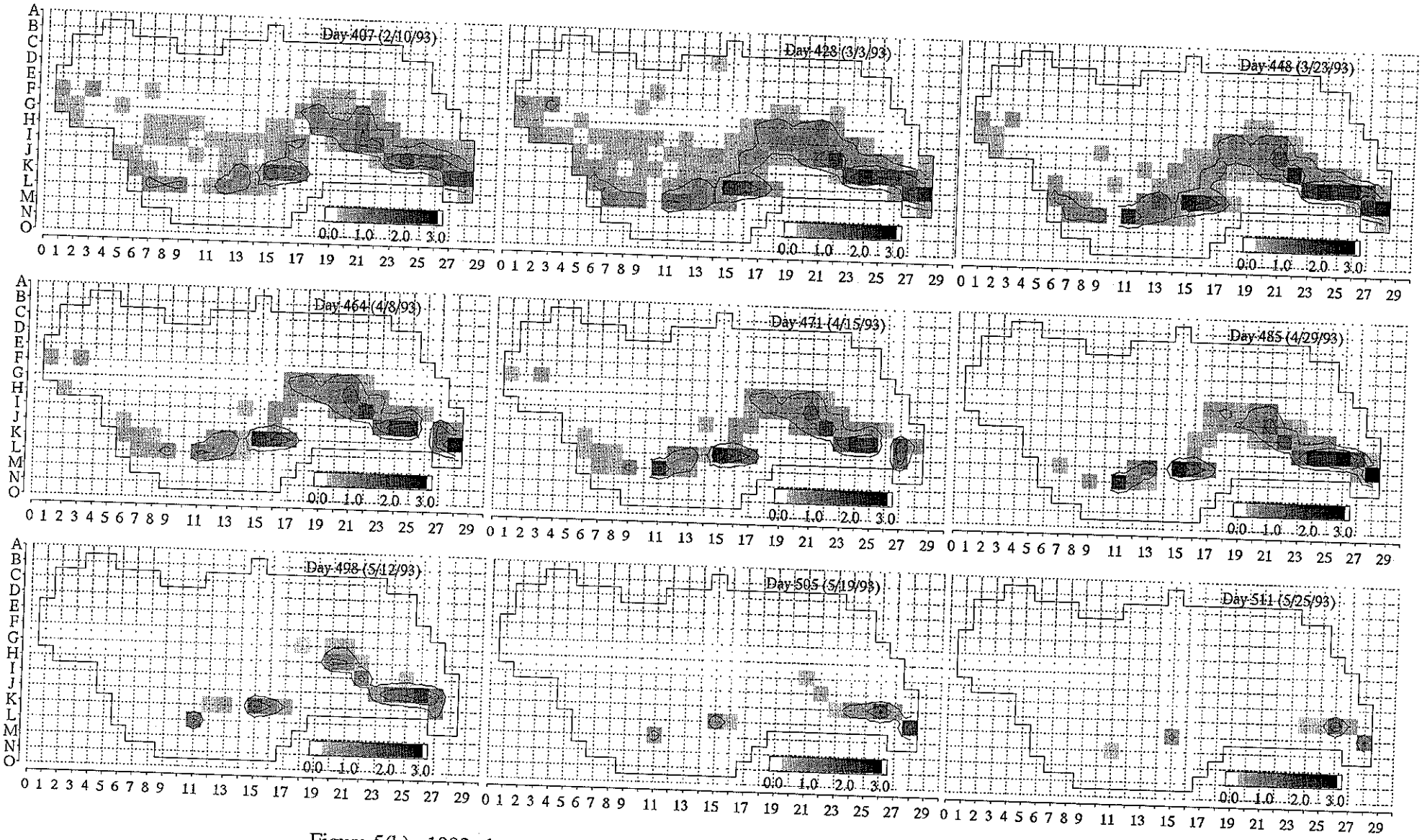

Figure 5(b). 1993 observed snow water equivalence maps. 0.5 m contour interval.

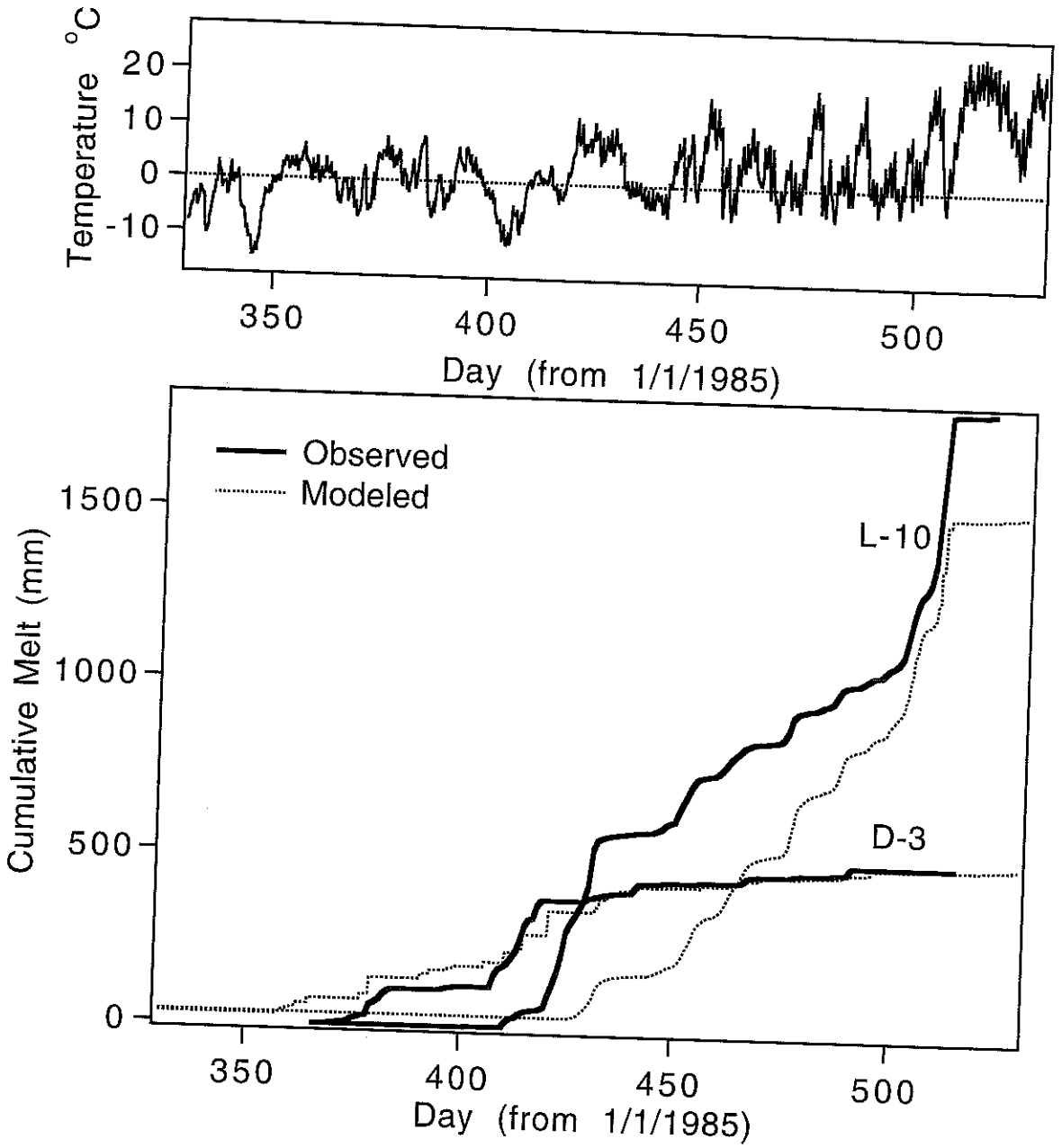

Figure 6. 1985-6 season cumulative snowmelt measured and simulated at sites D3 and L-10.

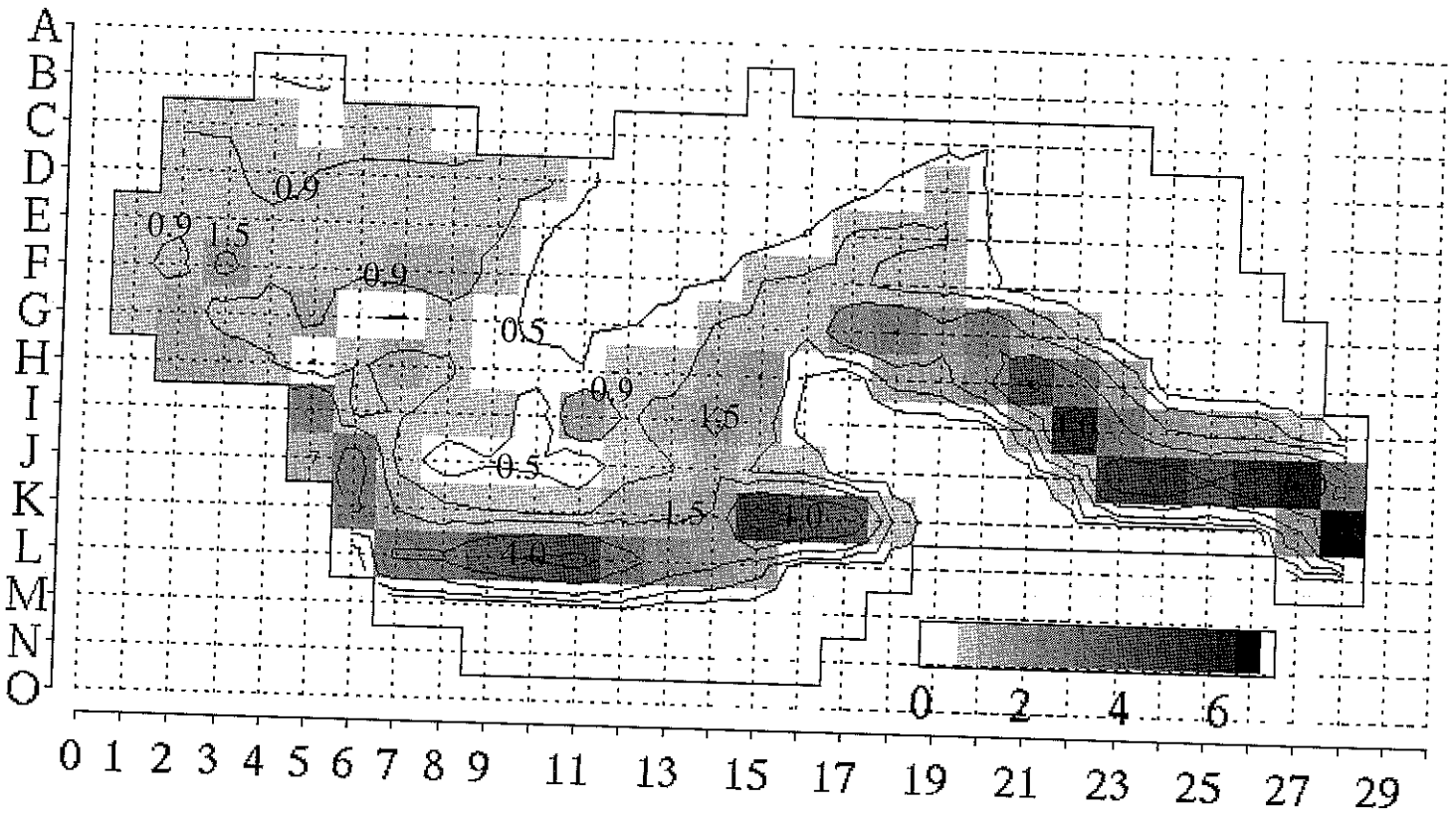

Figure 7. Weighted average drift factors. Contours at 0.5, 0.9, 1.5, 2.5, 4 and 6.

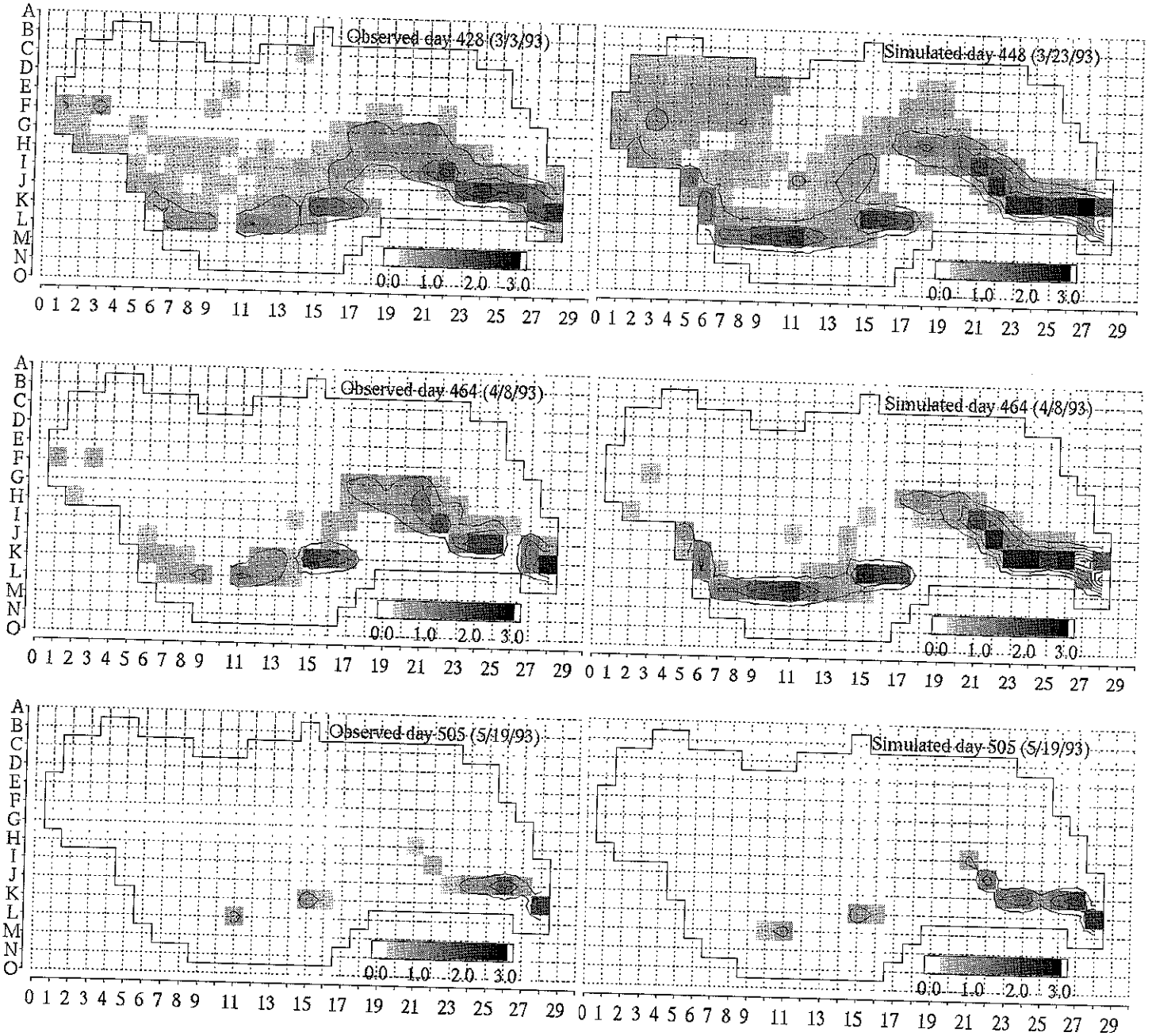

Figure 8. Observed and simulated snow water equivalence maps.

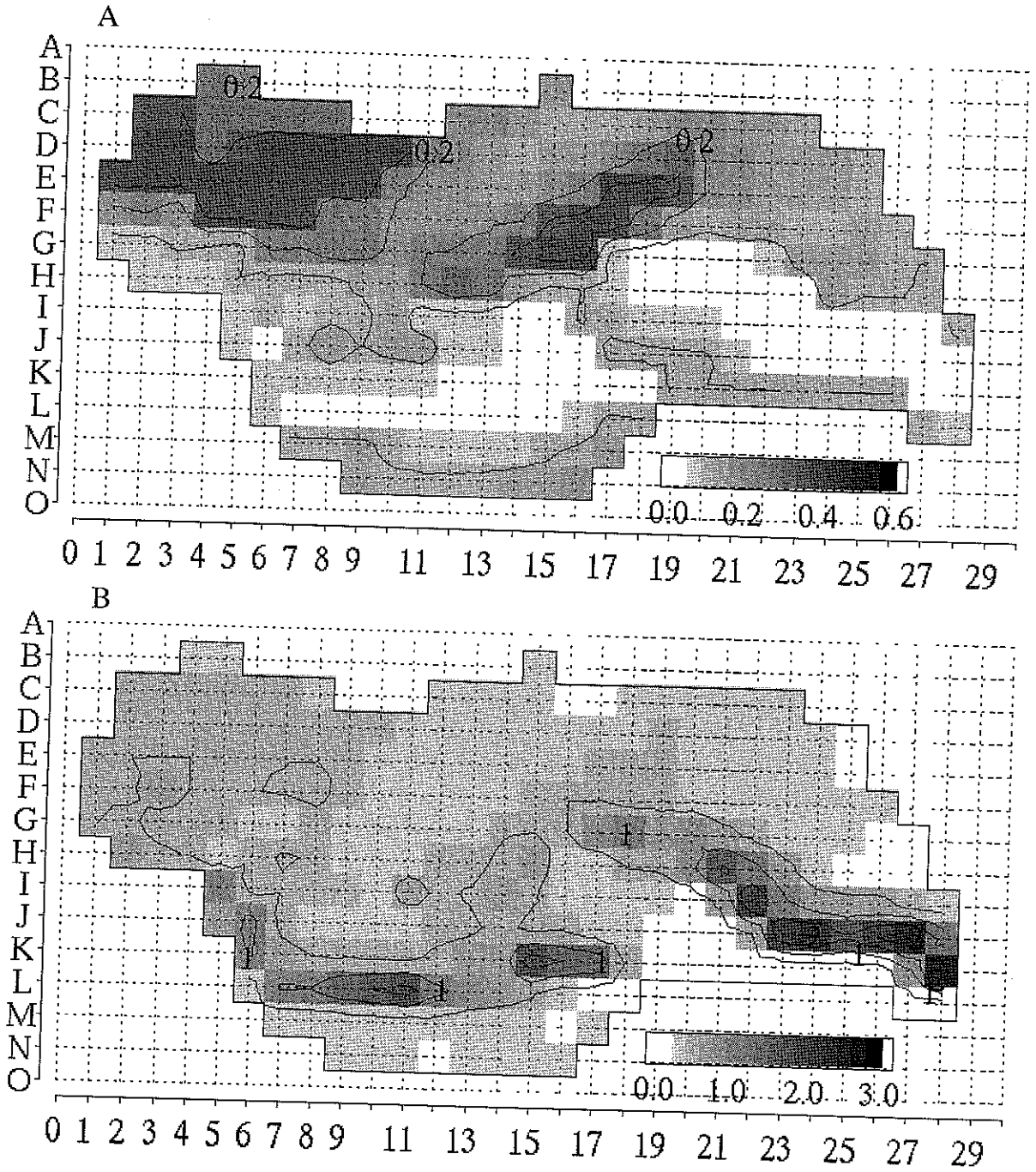

Figure 9. Total simulated surface water input (rain + snowmelt) a) October 29, 1985 to February 25, 1986 and b) October 29, 1985 to July 4, 1986. Contours in m.

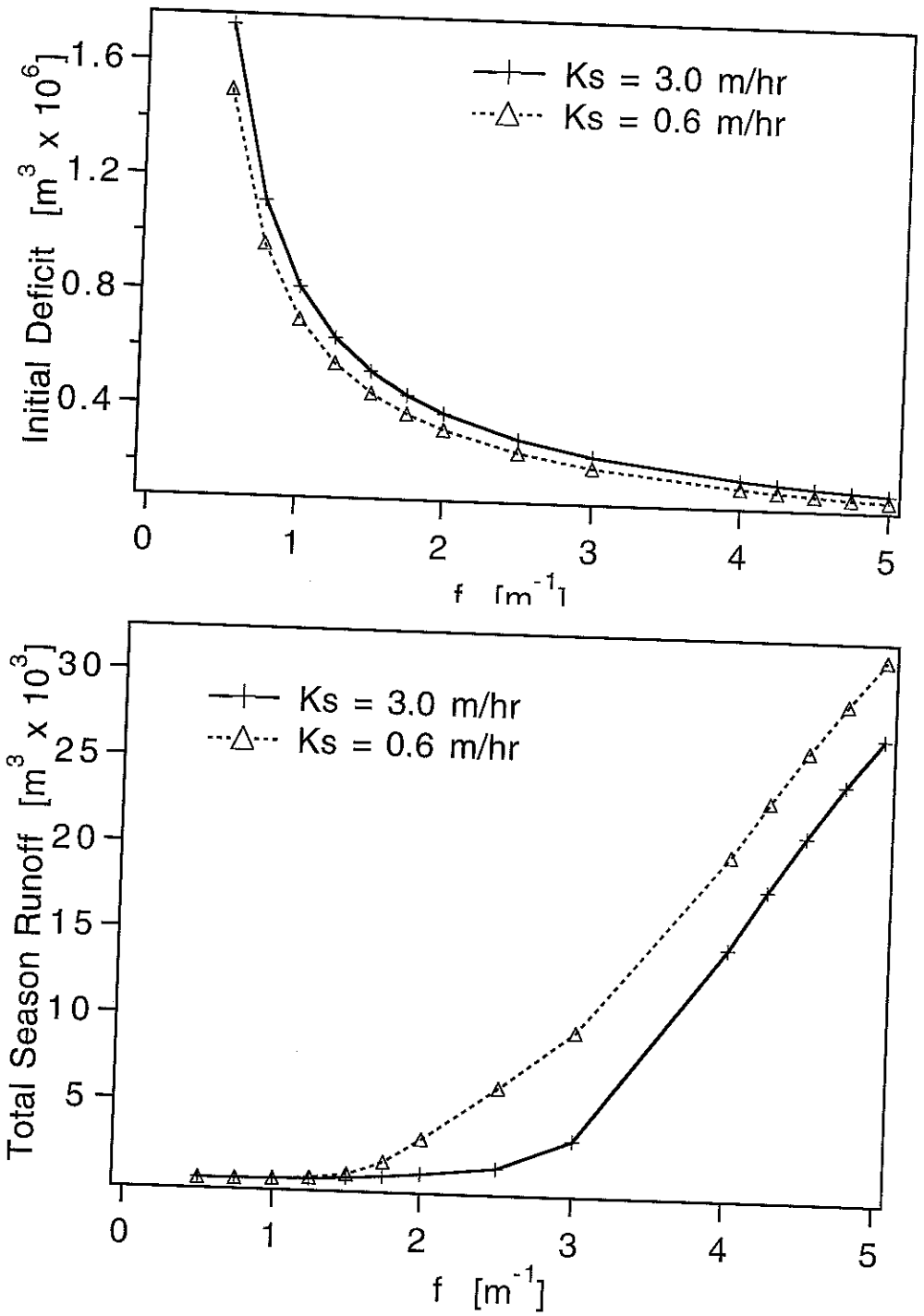

Figure 10. Initial deficit and total season runoff for a homogeneous catchment as a function of k_s and f.

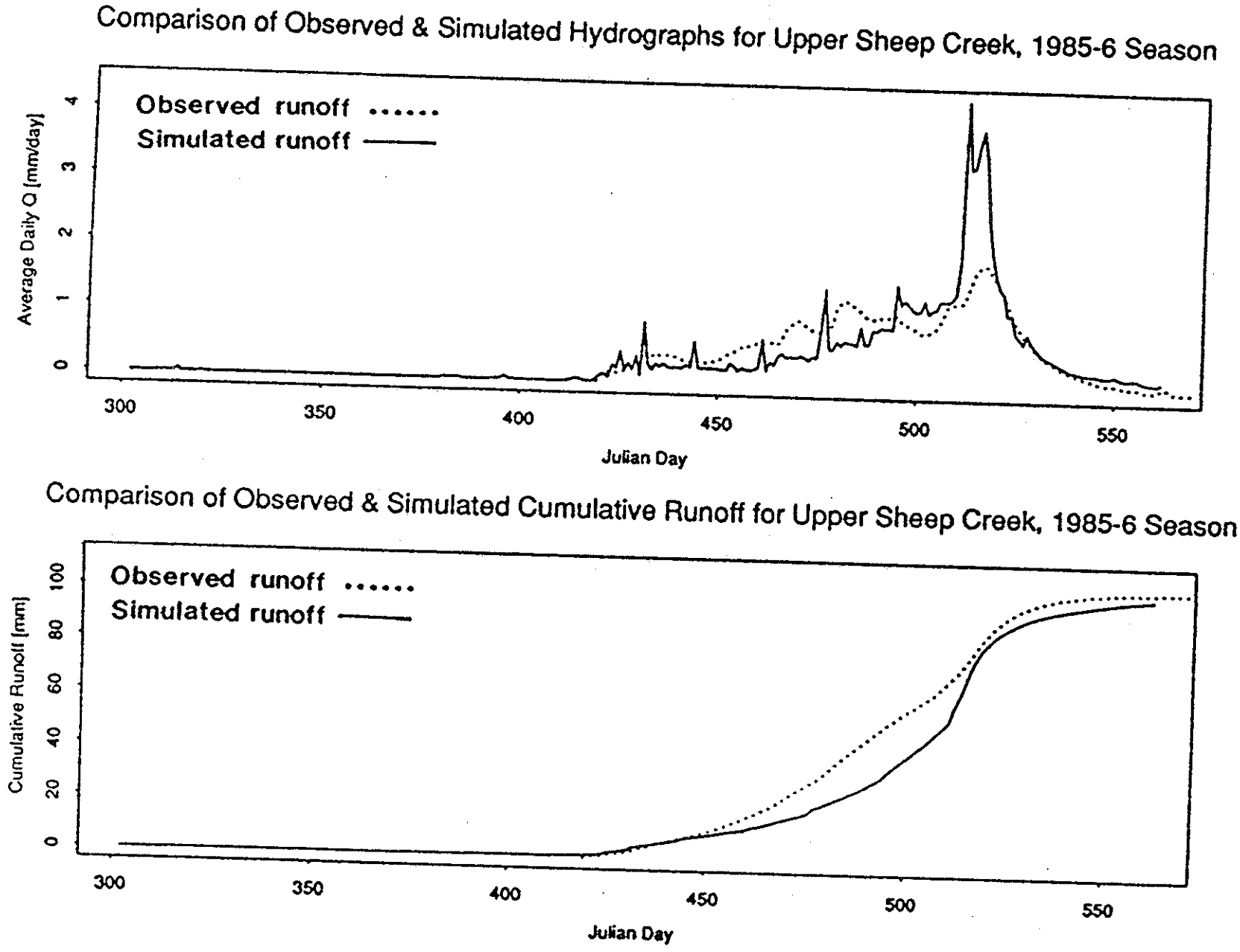

Figure 11. Cumulative and daily average outflow hydrographs for the 1985-6 snow season at Upper Sheep Creek with uniform parameters.

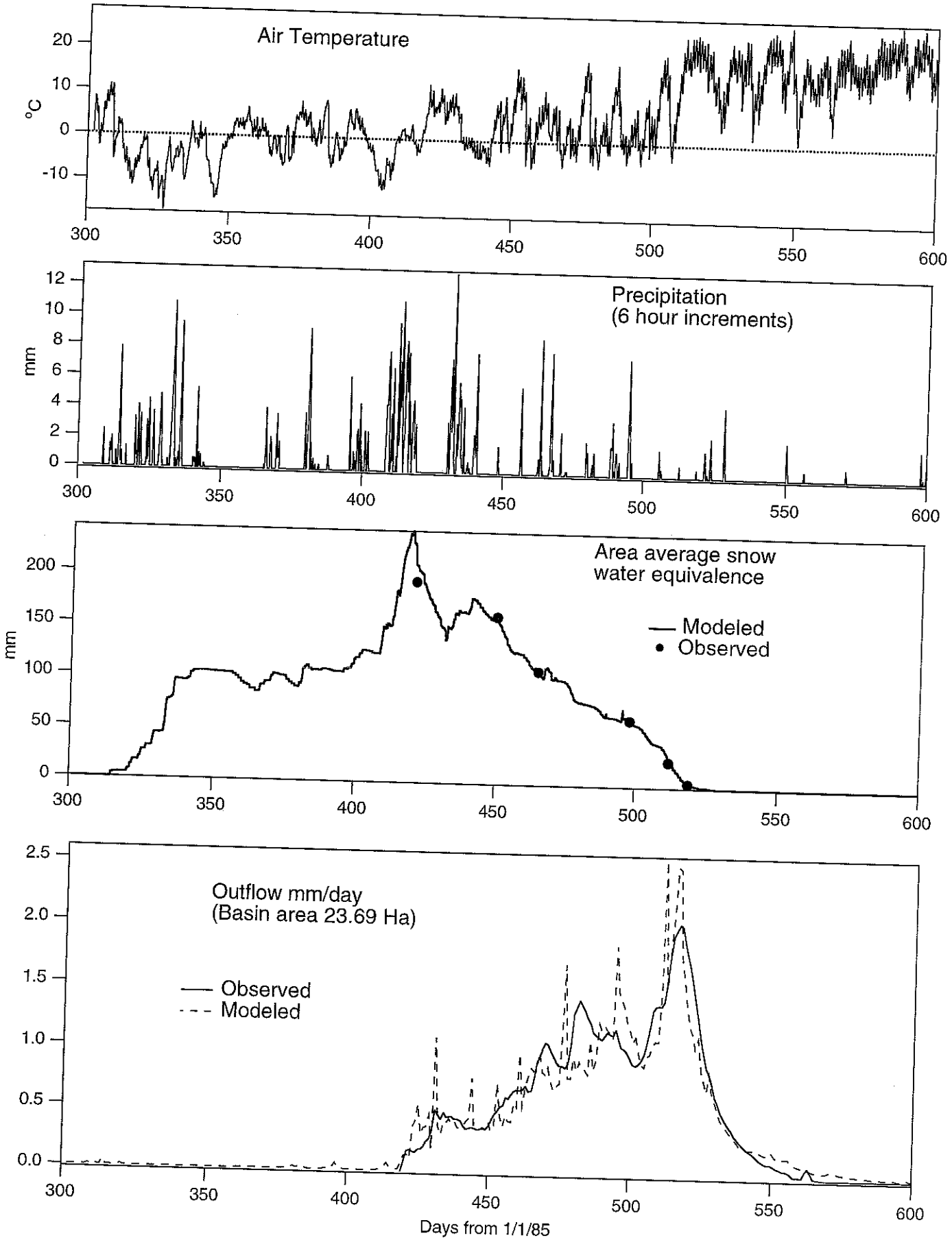

Figure 12. 1985-6 hydrograph and climate inputs for final parameter set. Parameters are k_s = 3 m/hr and f = 4.75, 5.15, 5.15, 2.9 and 2.7 for soil types GaG, HmG, GfF HbF and GfG respectively.

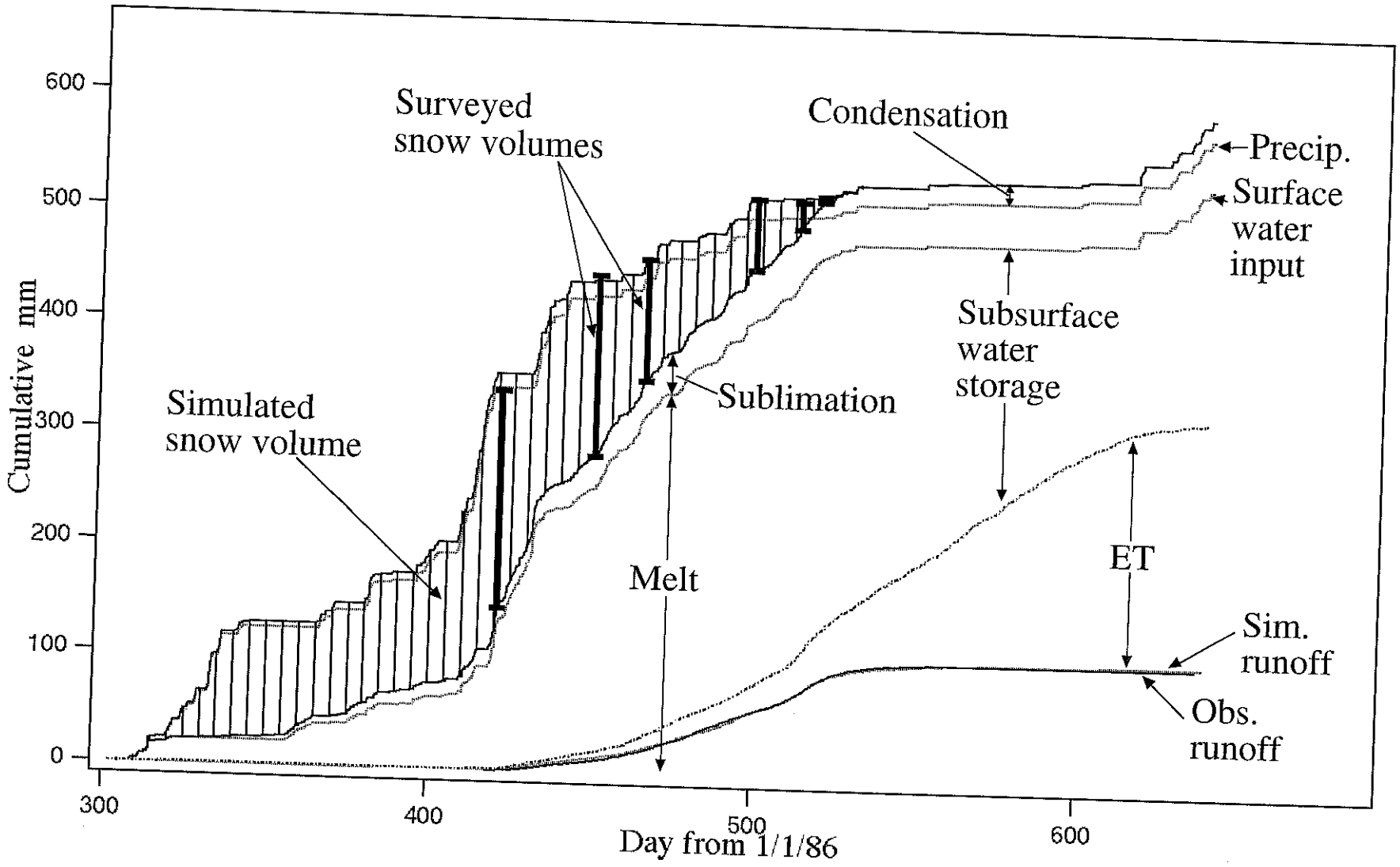

Figure 13. Cumulative overall mass balance 1985-6.

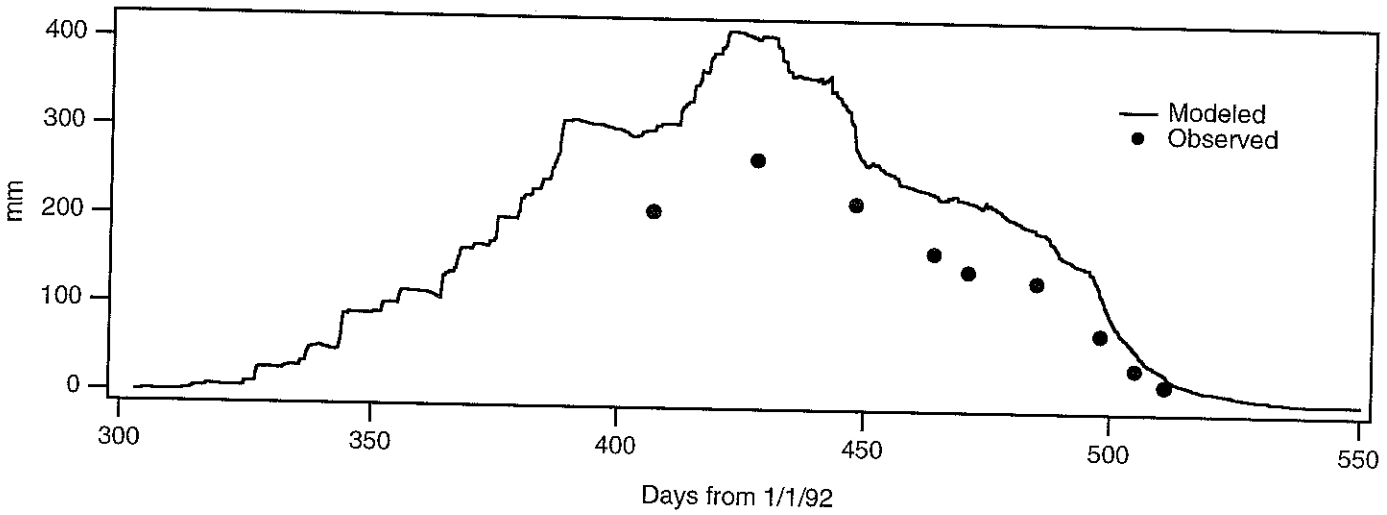

Figure 14. Area average snow water equivalence.

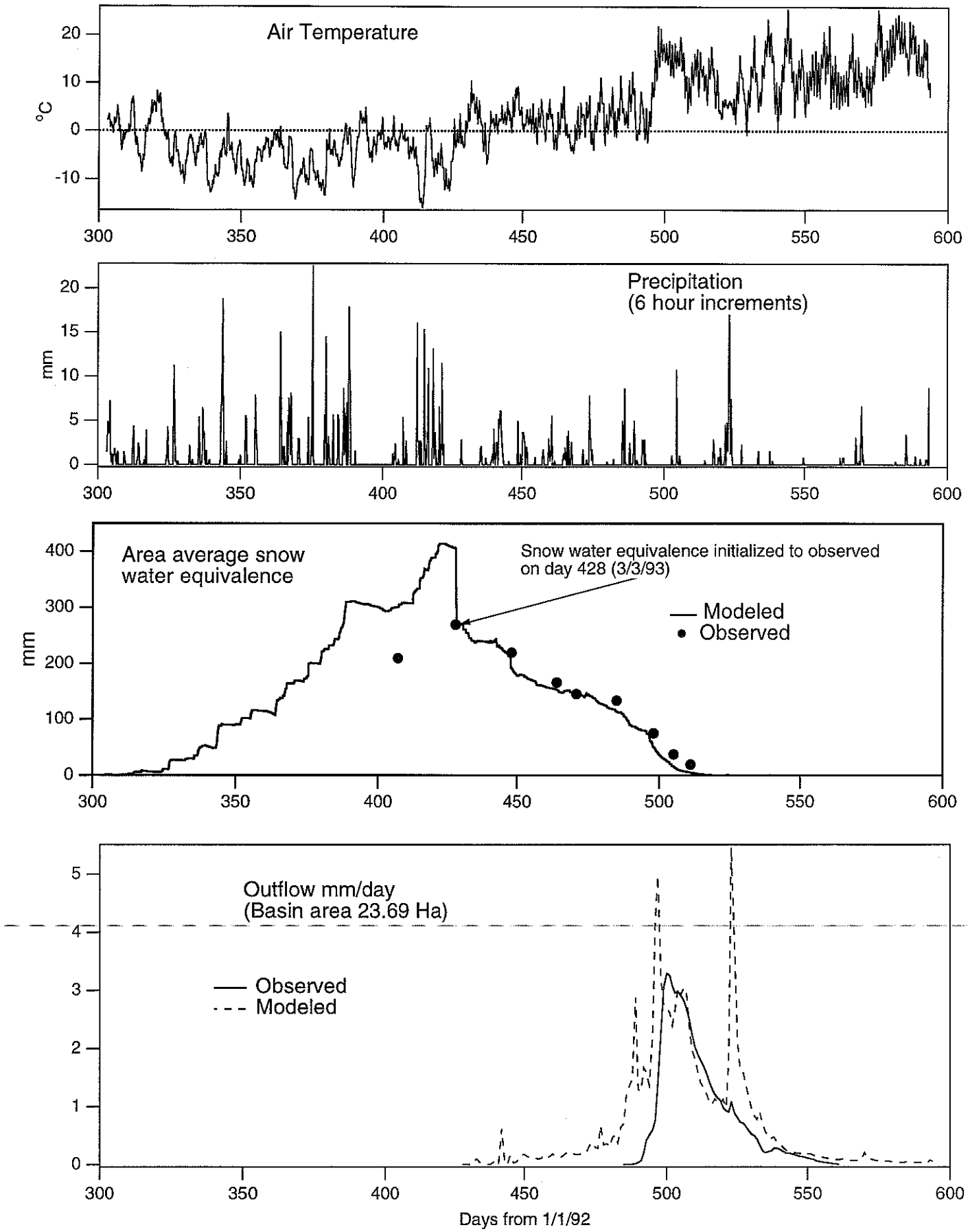

Figure 15. 1992-3 hydrograph and climate inputs.
Parameters are as for figure 13, 1985-6 data.

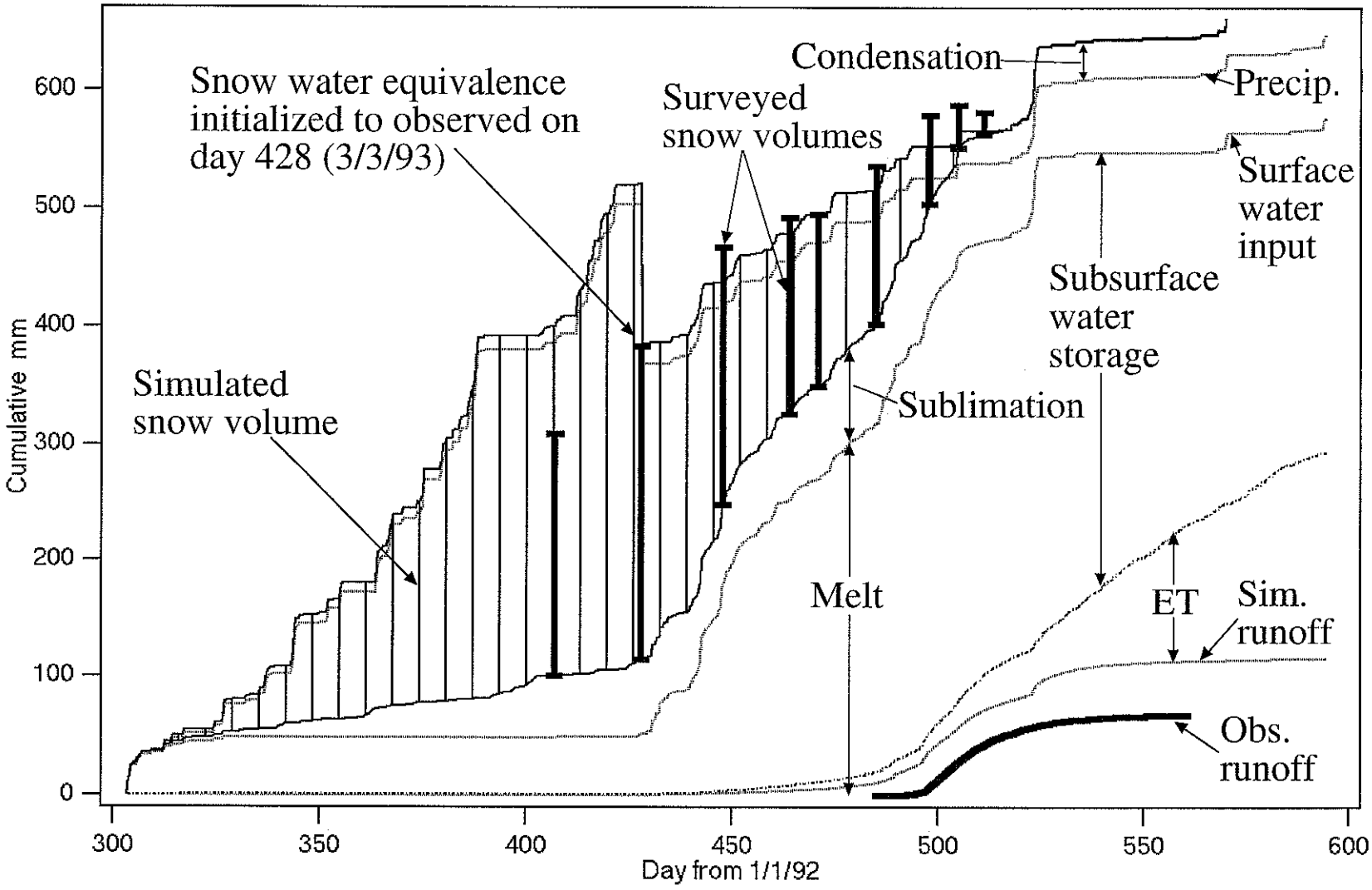

Figure 16. Cumulative overall mass balance 1992-3.